HHS Public Access

Author manuscript

*Neurobiol Dis*. Author manuscript; available in PMC 2023 November 01.

Published in final edited form as:

*Neurobiol Dis*. 2022 November ; 174: 105887. doi:10.1016/j.nbd.2022.105887.

# Alzheimer's disease/dementia-associated brain pathology in aging DPP6-KO mice

**Lin Lin**[1,*], **Ronald S. Petralia**[2,*], **Lynne Holtzclaw**[1], **Ya-Xian Wang**[2], **Daniel Abebe**[1], **Dax A. Hoffman**[1]

[1]Molecular Neurophysiology and Biophysics Section, Program in Developmental Neuroscience, *Eunice Kennedy Shriver* National Institute of Child Health and Human Development,

[2]Advanced Imaging Core, National Institute on Deafness and Other Communication Disorders, National Institutes of Health, Bethesda, MD 20892, USA.

## Abstract

We have previously reported that the single transmembrane protein Dipeptidyl Peptidase Like 6 (DPP6) impacts neuronal and synaptic development. DPP6-KO mice are impaired in hippocampal-dependent learning and memory and exhibit smaller brain size. Recently, we have described novel structures in hippocampal area CA1 in aging mice, apparently derived from degenerating presynaptic terminals, that are significantly more prevalent in DPP6-KO mice compared to WT mice of the same age and that these structures were observed earlier in development in DPP6-KO mice. These novel structures appear as clusters of large puncta that colocalize NeuN, synaptophysin, and chromogranin A, and also partially label for MAP2, amyloid β, APP, α-synuclein, and phosphorylated tau, with synapsin-1 and VGluT1 labeling on their periphery. In this current study, using immunofluorescence and electron microscopy, we confirm that both APP and amyloid β are prevalent in these structures; and we show with immunofluorescence the presence of similar structures in humans with Alzheimer's disease. Here we also found evidence that aging DPP6-KO mutants show additional changes related to Alzheimer's disease. We used *in vivo* MRI to show reduced size of the DPP6-KO brain and hippocampus. Aging DPP6-KO hippocampi contained fewer total neurons and greater neuron death and had diagnostic biomarkers of Alzheimer's disease present including accumulation of amyloid β and APP and increase in expression of hyper-phosphorylated tau. The amyloid β and phosphorylated tau pathologies were associated with neuroinflammation characterized by increases in microglia and astrocytes. And

**Address correspondence to:** Dax Hoffman, 35 Lincoln Drive, MSC 3715, Building 35, Room 3C-905, Bethesda, MD 20892-3715; hoffmand@mail.nih.gov.

*Equal contribution authorship

Lin Lin: Conceptualization, Investigation, Writing - Original Draft Writing - Review & Editing, Visualization, Project administration
Ronald S. Petralia: Conceptualization, Investigation, Writing - Original Draft Writing - Review & Editing, Visualization, Project administration, Funding acquisition
Lynne Holtzclaw: Investigation
Ya-Xian Wang: Investigation
Daniel Abebe: Investigation
Dax A. Hoffman: Conceptualization, Investigation, Writing - Original Draft Writing - Review & Editing, Visualization, Project administration, Funding acquisitiong Visualization Project administration Funding acquisition

levels of proinflammatory or anti-inflammatory cytokines increased in aging DPP6-KO mice. We finally show that aging DPP6-KO mice display circadian dysfunction, a common symptom of Alzheimer's disease. Together these results indicate that aging DPP6-KO mice show symptoms of enhanced neurodegeneration reminiscent of dementia associated with a novel structure resulting from synapse loss and neuronal death. This study continues our laboratory's work in discerning the function of DPP6 and here provides compelling evidence of a direct role of DPP6 in Alzheimer's disease.

**Keywords**

DPP6; Alzheimer's disease; neurodegeneration; dementia; neuroinflammation; hyper-phosphorylated Tau; amyloid β plaques; APP

## INTRODUCTION

We have reported that DPP6, a single transmembrane protein that is highly expressed in the hippocampal regions of the brain (Strop et al., 2004; Lin et al., 2014; Malloy et al., 2022), plays a novel role to impact neuronal and synaptic development (Lin et al., 2013), in addition to its previously described role as an auxiliary subunit of the Kv4 of voltage-gated $K^+$ channels (Nadal et al., 2003), impacting neuronal excitability and plasticity (Hoffman et al., 1997; Sun et al., 2011). Recently we have discovered a novel NeuN+ structure in hippocampal region CA1 in aging mice that is significantly more prevalent in aging DPP6-KO mice compared to WT. The novel structures appear as clusters of large puncta that are abnormal presynaptic swellings and associate with a number of markers for aging and Alzheimer's disease (AD) (Lin et al., 2020; Malloy et al., 2022).

AD is a degenerative brain disease characterized by memory impairment and cognitive decline that can affect behavior, speech, visuospatial orientation, motor functions, and circadian rhythms (DeTure and Dickson, 2019; Egger et al., 2014). It is the most common form of dementia, and it may be mixed with other causes of dementia such as vascular dementia and Lewy body dementia (DeTure and Dickson, 2019). The brain of an AD patient often shows moderate cortical atrophy and decreased brain weight, and there is loss of synapses and neurons, but these changes are not specific to AD (DeTure and Dickson, 2019). Dominantly inherited familial AD is rare but may be caused by mutations in amyloid precursor protein (APP) or presenilin. Aging is the most common risk factor for AD, and a number of genetic risk factors have been implicated, such as the apolipoprotein E gene (DeTure and Dickson, 2019). AD is caused by complex brain changes following cell damage. It leads to dementia symptoms that gradually worsen over time (Caselli et al., 2017; Schultz et al., 2004). Diagnostic hallmarks include the abnormal accumulation of extracellular amyloid-β peptide (Aβ, amyloid plaques), intracellular neurofibrillary tangles composed of phosphorylated tau (phospho-tau), and neuronal loss. Autopsy studies show that most people with AD develop substantial Aβ amyloid plaques and phospho-tau tangles in the brain as they age (Gouras et al., 2000; Gyure et al., 2001). Amyloid plaques can be diffuse or dense core, with the latter sometimes associated with tau-positive or dystrophic neurites that can be labeled with various synaptic markers including APP (DeTure and

Dickson, 2019). Those with a dense core may be surrounded by an accumulation of APP with phospho-tau and presynaptic proteins, all presumably derived from presynaptic terminals (Jorda-Siquier et al., 2022). Aβ and phospho-tau pathologies are associated with neuroinflammation characterized by activation of microglia and astrocytes and elevated levels of proinflammatory cytokines (Osborn et al., 2016; Spanic et al., 2019).

The DPP6 gene, which is from the 7q36 locus, has been reported to be associated with numerous intellectual and neurodevelopmental disorders (Marshall et al., 2008; Liao et al., 2013; Egger et al., 2014; Bock et al., 2016; Prontera et al., 2014; Noor et al., 2010; Maussion et al., 2017; Rahman et al., 2019; Naujock et al., 2020; Zhang et al., 2021; Liu et al., 2020). 7q36 first was identified as a novel locus for AD by Rademakers et al. (Rademakers et al., 2005); they noted the presence of the DPP6 gene at the locus although the involvement of DPP6 in AD was not clear in this early study. Cacace et al. reported in 2019 that DPP6 is involved in dementia with enhanced rare variants and nonsense mutations, and in early onset AD and frontotemporal dementia (FTD) with frameshift and missense mutations (Cacace et al., 2019). They also found evidence for reductions in DPP6 RNA and protein in the brain from patients that carry rare DPP6 missense variants. Overall, they found that the reduction of DPP6 expression and function can have a high impact in dementia, although the association of DPP6 and dementia is not clear in all cases (Kirola et al., 2021; Cacace et al., 2021). Another report found a specific late reduction of DPP6 in the olfactory bulb in AD patients who were diagnosed with advanced progression as per NIA-AA criteria, and where neuritic tangles were found in the olfactory bulb at this stage (Zelaya et al., 2015; Jack et al., 2012 for NIA-AA criteria).

In this study, we characterized changes in cell architecture and proteins associated with aging in the hippocampus of DPP6-KO mice. We found hippocampi of aging DPP6-KO mice to be smaller than WT in *in vivo* MRI studies, with signs of neuronal loss and atrophy, and immunocytochemical and biochemical evidence for an increase in phospho-tau proteins and greater gliosis. We also found Aβ amyloid and amyloid-precursor protein (APP) associated with the clusters of large NeuN+-labeled puncta; furthermore, we found evidence of similar clusters of NeuN+ puncta in the CA1-hippocampus region in human donors with AD. Our findings demonstrate that DPP6, in addition to its effects on early synapse development, appears to be important for the maintenance of synaptic function during aging, as its loss leads to learning and memory deficits associated with physical and biochemical markers for dementia. Overall, this study builds on our previous work on DPP6 in synaptic function in development, especially as related to potassium channels, and further develops the important role of DPP6 in neuronal and synaptic function in late aging that we first described in Lin et al. (2020). Here we extend these studies to provide for the first time, a strong link between DPP6 and AD.

## MATERIALS AND METHODS

### Animals

WT and DPP6-KO mice were genotyped by PCR after being weaned at 21 day old. WT background was C5BL/6, as it was for DPP6-KO mice. Mice were housed under a 12-h light/dark cycle with the lights turned off at 18:00. All animal procedures were performed

in accordance with NIH guidelines that were approved by the National Institute of Child Health and Human Development Animal Care and Use Committee.

## Human brain tissue

The human brain sections, which included the CA1 hippocampal region, were obtained from the NIH NeuroBioBank, and included brains from 4 patients with AD and 4 controls. Donor 1 (S10727) was a 64-year-old male with AD - Braak stage V/VI (post-mortem interval (PMI): 8.5 hours)); donor 2 (3566) was a 74-year-old female with late onset AD (Braak stage not recorded; PMI: 11.92 hours); donor 3 (94517) was a 74-year-old male with late onset AD - Braak stage VI (PMI: 6.25 hours); donor 4 (S14331) was a 74-year-old male with AD, Braak and Braak tangle stage VI/VI with a high probability of dementia due to AD (PMI: 22 hours); donor 5 (S12545) was a 69-year-old male with neurofibrillary degeneration and mild atherosclerosis and arteriosclerosis, and served as a control (PMI: 18.43 hours); donor 6 (6280) was a 65-year-old male (PMI: 23 hours); donor 7 (S11774) was a 74-year-old male (PMI: 15 hours); donor 8 (S16640) was a 70-year-old male (PMI: 15 hours); donors 6–8 served as controls since neuropathological assessment revealed no neuropathology diagnosis. Quality of sections, fixation, and labeling varied somewhat among donors, likely due to the inherent problem of using human tissue, since it only can be fixed after substantial PMIs.

## Electron microscopy

Hippocampi were prepared for transmission electron microscope (TEM) study as described previously (Li et al., 2017; Lin et al., 2020). Briefly, 12-month-old WT and DPP6-KO mice were fixed and embedded in epon. Thin sections (60 nm) were examined in a JEOL JEM2100 TEM (Peabody, MA). Images were taken from 2 WT and 2 KO mice. To quantify invaginating structures at synapses, we counted 3 categories. The first, “spine invaginations,” included any type of invaginating structure in a presynaptic terminal forming a synapse with a postsynaptic spine in the image. The second, “two-terminal invaginations,” included invaginations in which clusters of presynaptic vesicles were found on both processes that invaginated with each other, indicating that both are derived from presynaptic terminals. These included a subset of counts from the first category of “spine invaginations’” as well as cases in which neither of the two invaginating processes could be traced to a spine synapse within the image. Finally, a third category, “total invaginations,” included all invaginating synapses that were counted in either or both of the first two categories, as well as any other kinds of terminal invaginations in which the processes were not traced to a synapse on a spine visible in the image.

Mouse hippocampi used for postembedding immunogold localization were prepared as described previously (Petralia et al., 2010; Sun et al., 2011; Lin et al., 2018; Lin et al., 2020; Petralia and Wang, 2021). Briefly, 12-month-old WT and DPP6-KO mice were fixed and brains were frozen in a Leica EM CPC (Vienna, Austria), and embedded in Lowicryl resin in a Leica AFS freeze-substitution instrument. Thin sections were labeled with primary antibodies and then incubated with immunogold-conjugated secondary antibodies (Ted Pella, Redding, CA, USA) and stained with uranyl acetate and lead citrate. For double-

immunogold labeling, we incubated the 2 primary antibodies together (same for the 2 secondary immunogold antibodies).

Two mice each from WT and DPP6-KO were studied for NeuN (1:35, rabbit, MilliporeSigma) and NeuN (1:35 or 1:50, mouse, Millipore) antibodies, and for antibodies to APP (1:7 or 1:25, rabbit, Abcam) and Aβ-amyloid (1:7, mouse, BioLegend). NeuN immunogold labeling was studied in double labeling with APP or Aβ. As noted in Lin et al., 2020, additional immunogold studies with antibodies to AT8 (1:25, mouse, Thermo Fisher), Tau3C (1:50, mouse, Thermo Fisher), and another synaptophysin (1:7, SP15, mouse, MilliporeSigma) produced only rare (background) gold labeling; these were used as controls for the immunogold technique. $NeuN^+$ swellings were difficult to find because of their scattered distribution. APP at 1:25 was used for quantitative immunogold studies of synapses in the CA1 neuropil. Double labeling with APP (1:7; rabbit) and NeuN (1:35: mouse) or with Aβ (1:7; mouse) and NeuN (1:35: rabbit) was used to study distribution in the NeuN+ swellings.

## Live mouse MRI procedures

Magnetic Resonance Imaging (MRI) was performed in the Mouse Imaging Facility (MIF) at NIH. Ten-month-old mouse was placed under general anesthesia in an induction chamber with an oxygen-enhanced air gas mixture containing 3–5% isoflurane. After anesthesia was induced (indicated by loss of righting reflex, decreased respiratory rate and non-responsiveness to gentle toe pinch of the hind limb with finger and thumb), the mouse was placed either supine or prone on a plastic cradle. The isoflurane was reduced to 1–2%, and the animals were maintained via nose cone. Isoflurane was scavenged using an in-house anesthetic gas vacuum scavenging system. Subcutaneous 0.9% saline (~0.5–1.0 ml/25 g mouse IP, SC) was given to maintain hydration. Sterile ophthalmic ointment was applied to the corneas to prevent desiccation under anesthesia.

The head of the anesthetized mouse was restrained in a plastic head-holder consisting of a bite bar and nosecone in a configuration similar to commercial stereotaxic devices. Blunt-tipped earpieces (coated with 2% lidocaine gel) were used as needed and were applied by trained personnel. A pressure transducer for respiratory detection was placed on the abdomen. Lightly adhesive tape (3M Transpore) was used as needed to stabilize the position of the animal. A fiber optic or standard temperature probe was placed rectally. To maintain body temperature, a circulating warm water pad was placed around the cradle. Some custom cradles had circulating warm water in the animal platform. Alternatively, a warm air blower was placed at the magnet bore. If needed, conductive leads were placed for the detection of the Electrocardiogram (ECG); a pulse oximeter was used optionally. The respiration waveform and rate (and ECG) were read on a computer monitoring/gating system. Respiration and temperature were monitored throughout the experiment for maintenance of anesthesia. MRI was performed for up to 3 h; typical scans were 30–90 min.

For survival studies, the mouse recovered in a clean cage or transport box on a circulating warm water heating pad. It was visually monitored until awake and ambulatory. Animals were transported back to their home facility in NIH-approved transport boxes or were housed overnight in the MIF.

## Cytokine Array

Mouse bleeds were collected in EDTA-treated tubes. These tubes were centrifuged at 1000 × g for 10 min at 4°C within 30 minutes of blood collection, and the supernatant (plasma) was collected immediately and flash frozen. Plasma diluted 1:2 was used to detect cytokines and chemokines by use of the 31-Plex Cytokine/Chemokine array (Eve Technologies).

## Immunofluorescence in mouse and human sections

Mice were perfused with 4% paraformaldehyde (PFA) in PBS and then equilibrated in 30% sucrose for 24 h. A series of floating 30 μm or frozen 7 μm coronal sections were taken from a Bregma range of −1.955 to −2.095 mm. 3–5 mice were examined and similar number of sections, up to 4 per animal, were used in each IF experiment. Then, samples were incubated with the primary antibody at 4°C overnight and then for 1 h at RT with fluorescent probe-conjugated secondary antibodies. Nuclei were labeled with DAPI. For human hippocampal sections, we performed antigen retrieval (AR) where slides were immersed into the antigen retrieval buffer (10 mM Sodium Citrate, pH 6.0). The buffer was heated on a hot plate or water bath to 95–100°C, and slides were immersed into the solution for 10 min. Then the buffer was allowed to cool to room temperature for 20 min and the slides were removed and we proceeded immediately with the blocking step, not allowing the slides to dry out. The permeabilization/blocking buffer was 0.3% TritonX-100+1% normal goat serum in 1x PBS. Then sections were incubated overnight with the primary antibody at 4°C following by the fluorescent probe-conjugated secondary antibodies as on the mouse brain sections. Immunofluorescence (IF)-labeled slides were imaged using either a Zeiss 710 or 880 confocal microscope, while entire brain section or just the hippocampus was scanned with a Carl Zeiss AxioScan.Z1 slide scanner, which had a 20× objective (Plan-Apochromat, NA 0.8) and a Colibri7 LED illumination source.

IF intensity and surface area measurements were taken and analyzed in ImageJ. Areas of either all brain sections, hippocampi or somas in the image were measured by using the computer mouse to draw along the area, and then measuring the surface area and mean intensity of the area. To measure the number of microglia or astrocytes by ImageJ, first we traced the CA1 area (entire CA1 plus the molecular layer of the dentate gyrus) to get the total surface area, then set up a threshold to measure the number of cell bodies, then divided by the total surface area. To measure the size of microglia or astrocytes, we measured the surface area of microglia or astrocytes by changing the threshold to include the cell processes, and then comparing the thresholded image to the raw image to make sure that each surface area measurement was from a single cell. Statistical analyses were performed using GraphPad Prism 9 by Student’s t-test.

## H&E and Bielschowsky staining

H&E staining: The unstained slides were deparaffinized in xylene, then hydrated through graded alcohols, 50 ml of 100% EtOH 2 times, 95% EtOH 1 time, 70% EtOH 1 time, and 50% EtOH 1 time, and then placed in running cold tap water to rinse. Then they were put in Carazzi’s hematoxylin, washed in tap water, and then put in one change of 95% ethanol. From there they were put in eosin-phloxine solution, and then run through graded alcohols to xylene. After xylene, the stained slides were coverslipped using Permount as

the mounting media. Bielschowsky staining: The unstained slides were deparaffinized in xylene, then hydrated through graded alcohols up to water. Then they were rinsed well in distilled water before being transferred to silver nitrate. Slides were then transferred to distilled water. After distilled water, the slides were placed in an ammoniacal silver solution for developing. Slides were washed in ammonium hydroxide, then washed in distilled water, and placed in sodium thiosulfate. Slides were rinsed in distilled water before being run through graded alcohols to xylene. After xylene, the stained slides were coverslipped using Permount as the mounting media.

## Tissue lysates and Western blots

Twelve-month old C57BL/6 WT and DPP6-KO mouse hippocampi were removed and lysed in lysis buffer (NaCl 150 mM, Tris-HCl 20 mM, 1% CHAPS (Sigma)): we added 1 tablet of Complete mini protease inhibitor cocktail, EDTA-free (Millipore Sigma) to 10 ml of basic lysis buffer, and 1x Halt Protease Inhibitor Cocktail (100x) (Thermo Scientific), and incubated for 20 min on ice, then sonicated 5 times for 5 s each. The lysate was centrifuged at 15,000x g for 20 min at 4°C, and the protein concentration of the lysate was measured by the Pierce™ BCA assay (Thermo Fisher). Equal amounts of protein were separated by electrophoresis on NuPAGE™ 10% Bis-Tris or 3–8% Tris-Acetate gels (Thermo Fisher) and transferred to PVDF membranes. The separated proteins were immunoblotted using APP, beta-Amyloid, alpha-Synuclein, P19ARF, and Actin-beta antibodies (please see the antibodies list for dilutions) and visualized by Alexa Fluor 680 secondary antibody (1:10,000, Invitrogen) and Alexa Fluor 800 secondary antibody (1:5,000, Rockland). Immunoreactivity was detected with the Odyssey infrared imaging system (LI-COR Biosciences, Lincoln, NE). Quantification of results was performed using Odyssey software (LI-CORBiosciences).

## Antibodies

| Name | Species | Company | Catalog# | IHC | WB |
|---|---|---|---|---|---|
| Actin-beta | Mouse | Sigma | A-1978 | | 1:10,000 |
| Actin-beta | Rabbit | Abcam | Ab-8227 | | 1:8000 |
| Amyloid Precursor Protein | Rabbit | Abcam | ab32136 | 1:500 | 1:10,000 |
| beta-Amyloid 1–16 | Mouse | BioLegend | 803001 | 1:1000 | |
| beta-Amyloid 1–42 | Rabbit | MilliporeSigma | Ab5078P | 1:400 | 1:1000 |
| alpha-Synuclein | Rabbit | Novus | NBP2-15365 | 1:400 | 1:1000 |
| Cleaved Caspase-3 (CC3) | Rabbit | Abcam | Ab2302 | 1:500 | |
| DPP6 | Rabbit | Abcam | ab41811 | | 1:2000 |
| GFAP | Rabbit | DAKO | Z033429-2 | 1:2000 | 1:10,000 |
| Iba1 (ICC IHC) | Rabbit | Wako | 019-19741 | 1:800 | |
| MAP-2 | Mouse | Millipore | MAB-3418 | 1:500 | |
| MAP-2 | Rabbit | Millipore | Ab-5622 | 1:500 | |
| NeuN | Mouse | Millipore | MAB377 | 1:1000 | 1:5000 |
| NeuN | Rabbit | MilliporeSigma | ABN78 | 1:500 | |

| Name | Species | Company | Catalog# | IHC | WB |
|---|---|---|---|---|---|
| P19ARF | Rabbit | Thermo Fisher | PA1-30670 | 1:100 | 1:1000 |
| Synaptophysin | Mouse | Sigma | S-5768 | 1:500 | |
| Synaptophysin (SP15) | Mouse | MilliporeSigma | MAB239 | For EM | |
| Tau-5 | Mouse | Biosource | AHB-0042 | 1:100 | 1:2000 |
| TauC3 (cleaved Asp421+422) | mouse | Thermo Fisher | AHB0061 | 1:200 | 1:2000 |
| PHF-Tau at Thr231 (AT180) | Mouse | Thermo Fisher | MN1040 | 1:200 | 1:2000 |
| PHF-Tau at Ser 202+Thr205 (AT8) | Mouse | Thermo Fisher | MN1020 | 1:300 | 1:2000 |

### Home Cage task

Locomotor activity-monitoring in a familiar environment was assessed over 6 days in individual home cages under normal vivarium conditioning via the photocell-based Photobeam Activity System version 2 (San Diego Instruments, San Diego, CA, USA). In this study, using 12-month-old WT and DPP6-KO mice, we performed the same 24-hour continuous locomotor activity monitoring in the home cage for 6 consecutive days. We used the Photobeam Activity System-Home Cage, in which locomotor activity is measured by quantifying the number of beam breaks during 24 hrs/6 days. It provided three measurements. One was Ambulation movement (XA+YA), which measures when the animal is breaking different beams. The second was Fine movement (XF+YF), which indicates that the animal is not moving and is repeatedly breaking the same beam. The third is Rear activity, when the animal is climbing.

### Statistical analysis

The n values and details of controls and comparisons used for statistical analyses are described for each experiment in the corresponding figure legends or within the Results section. Statistical analyses were performed using GraphPad Prism 9. We used Student's t-test or two-way ANOVA with Tukey's multiple comparisons. All results are presented as the mean±SEM.

## RESULTS

### Aging DPP6-KO mice lose hippocampal volume with neurodegeneration

Our previous studies found that adult DPP6-KO mice have problems in hippocampal synaptic development (Lin et al., 2013) and impaired memory and recognition and learning behaviors along with microcephaly (Lin et al., 2018). We found that DPP6-KO mice have significantly lower body and brain weight compared to WT, from early ages up to 6 months old. Following these findings, we sought to characterize aging DPP6-KO mice.

First, we examined WT versus DPP6-KO mice up to 12 months of age. This is considered middle age in WT mice when they show significant changes in behavior compared to younger mice (Shoji et al., 2016). We found that 12-month-old DPP6-KO mice have significantly lower body (Fig. 1A,B, $p < 0.0001$) and brain weight (Fig. 1C,D, $p < 0.0001$) compared to WT despite our confirmation that DPP6-KO mice have normal feeding

behavior, which was assessed by measuring the intake of food (data not shown - mice were put in a new cage and the amount of food left weighed every day at the same time for 7 days, checking for pellets left in the bedding). This is consistent with the trend shown in younger DPP6-KO mice where body weight was found to be significantly lower than WT from 1–6 months and brain weight at 3 and 6 months (Two-way ANOVA, $p < 0.0001$ in both body and brain weight) (Lin et al., 2018).

Previous studies have shown that hippocampal volume changes over time, and this has the potential to be a marker for AD and dementia subtypes (Vijayakumar A, Vijayakumar, 2013; Vermunt et al., 2018; den et al., 2010; Schuff et al., 2009; Maruszak A, Thuret S, 2014). Here we performed *in vivo* MRI scans of live, aging DPP6-KO mouse brains using a 9.4T MRI scanner system for small animal studies (Bruker, Germany). Two measurements were calculated to assess the volume of the mouse brain: absolute volume was measured in $mm^3$ and relative volume was measured as a percentage of the total brain volume. We found decreased total brain volume in aging DPP6-KO compared with WT (Fig. 1E,F, $p < 0.001$). Both absolute and relative volume of the hippocampal region were decreased in the mutant (Fig. 1G left: absolute volume $p < 0.0001$; right: relative volume $p < 0.0001$). These data are consistent with the decrease in brain weight (Fig. 1D, Lin et al., 2018). We performed immunofluorescence (IF) staining for the neuronal marker NeuN to test if the cause of the smaller volume of the hippocampus was due to a reduction in the total number and/or size of neurons. We found that the mean intensity of NeuN in hippocampus was lower in 12-month-old DPP6-KO mice brain sections (Fig. 1H,I, $p < 0.01$) than in WT. Neuronal soma labeling was less intense in the DPP6-KO. DAPI-colabeling to identify the neuronal nuclei also appeared to be less intense in the DPP6-KO sections compared to WT. IF with the apoptosis marker cleaved caspase 3 (CC3) showed greater labeling in the hippocampal region, especially in CA3 stratum pyramidale. We also found that the intensity of DAPI was significantly decreased in CA1 and CA3 stratum pyramidale, and NeuN intensity was significantly decreased in CA3 stratum pyramidale (data not shown) in 12-month-old DPP6-KO mice compared to WT (Fig. 1J,K), suggesting more cell death. We performed IF with NeuN and MAP2 to study neuronal morphology in hippocampal CA1 of 12-month DPP6-KO mice (4 sections per animal; Fig. 1L). In general, these neurons showed shrunken and abnormal somas, determined by measuring the soma surface area in the CA1 stratum pyramidale (Fig. 1M, $p < 0.0001$), and had fewer or more abnormal apical dendrites compared to WT, showing a lower intensity of MAP2 in the CA1 stratum radiatum (Fig. 1N, $p < 0.01$). Apical dendrites had an irregular shape compared to a straight profile in the WT. These results suggest that there is a decrease in the number of pyramidal neurons in DPP6-KO, paralleled by an increase in apoptosis causing a decrease brain size and hippocampal volume.

## APP accumulation in presynaptic terminals is associated with increased invaginations and with the novel NeuN+ swellings in aging DPP6-KO mice

Since it appears that the $NeuN^+$ swellings in the CA1 region at 12 months are derived from presynaptic terminals (Lin et al., 2020), the ultrastructure of definitive presynaptic terminals in the neuropil of the CA1 stratum radiatum was examined with TEM to determine if presynaptic terminals, especially those making synaptic contacts with dendritic spines in

the DPP6-KO show any modifications from WT. Both WT and DPP6-KO mice showed structures typical of presynaptic terminals including clusters of synaptic vesicles and mitochondria (Petralia et al., 2014) (Fig. 2A). Also, invaginating structures were common in presynaptic terminals of spine synapses of both WT and mutant. The profiles of these structures in the image were generally elongated and contained a diffuse matrix surrounded by a distinct double-membrane. Such invaginating structures may be derived from the postsynaptic spine, adjacent presynaptic terminal, or glial process; they can contribute to synapse development, maintenance, and plasticity, and can be especially elaborate in synapses mediating rapid signal integration (Petralia et al., 2015, 2018, 2021). Many of these also contained a cluster of vesicles identical to the synaptic vesicles within the terminal, and so appear to be derived from adjacent presynaptic terminals (Fig. 2A). Furthermore, often the section-profiles of these invaginations were continuous with adjacent terminals, so that the two adjacent terminal-profiles appeared to be intertwined; examples of the latter were seen both when the postsynaptic spine was in the section (arrows in Fig. 2A) and in other examples when only the two adjacent terminals were present in the section (not shown). In contrast to invaginations that could be traced definitively to adjacent presynaptic terminals, none of the other invaginations (e.g., lower left arrow in Fig. 2Ac) could be traced definitively in the section profiles to the spines or glial processes. This suggests that invaginations are derived most commonly from adjacent presynaptic terminals. An interesting exception here is seen in Figure 2Aa, in which one of the invaginating processes projects directly from a large dendrite and the terminal projects also into the dendrite.

Quantification showed that these invaginating structures in terminals, including those that could be identified as being derived from adjacent terminals, were more prevalent in the DPP6-KO compared to WT (Fig. 2C, $p < 0.001$). We then examined differences in immunogold localization of the presynaptic terminal protein, APP (Laßek et al., 2013; Weingarten et al., 2017), in the neuropil of the CA1 of WT and mutant. Note that in most cases, the reduction of quality of ultrastructure due to the preparation techniques for immunogold localization made it difficult to identify the invaginating structures noted above. In comparison, immunogold labeling for APP was prevalent in presynaptic terminals; in most images taken of the CA1 neuropil, all gold particles in identifiable structures were in presynaptic terminals (Fig. 2C). Quantification of the gold labeling for APP in the neuropil showed that labeling is higher in the DPP6-KO than in the WT (Fig. 2D, $p < 0.0001$). Gold-labeling in a separate study also confirmed that APP is present in the NeuN+ swellings from two DPP6-KO mice (Fig. 2E+F, G); gold labeling for APP was scattered throughout the swelling and including some prominent labeling in the outer portions of the NeuN+ swellings. This corresponded with IF of the NeuN+ large puncta showing some colocalization with small puncta for APP, most commonly in the outer portions of the NeuN+ puncta (Fig. 2G inset; also as noted in Lin et al., 2020). To confirm that APP is higher in the DPP6-KO than in the WT, we performed IF to label APP in 12-month-old brain sections, and we found that the APP intensity in DPP6-KO hippocampus was significantly higher than in WT (Fig. 2H,I, $p < 0.05$). We also found higher protein levels of APP in the DPP6-KO compared to WT in Western blot (Fig. 2J,K, $p < 0.01$). Thus, the increase in APP in the DPP6-KO hippocampus was corroborated with three different methods; and we

identify at least two significant changes in the presynaptic terminals in the 12-month mutant: increased terminal-terminal invaginations and increased APP.

## Amyloid accumulation in CA1 hippocampus of aging DPP6-KO mice

Given increased APP in DPP6-KO mice, we performed IF staining for Aβ in brain sections of 12-month-old mice using the well-characterized Aβ antibody (803001, BioLegend). As for APP, we found that the intensity of Aβ in the CA1 of the hippocampus was higher in DPP6-KO than in WT mice (Fig. 3A–C). Labeling in the neuropil of the stratum radiatum consisted of numerous, irregular puncta and some small somas (Fig. 3A) and there also were accumulations of labeling in cytoplasm of neurons of the stratum pyramidale (Fig. 3B). There was more abundant labeling overall in the hippocampus in the DPP6-KO than in the WT (Fig. 3C, $p < 0.001$). We examined the Aβ protein expression in hippocampal total lysate. Our western blots showed that Aβ exists in multiple forms including both low and relatively high molecular-weight forms. We found higher expression of all forms in hippocampal lysate in 12-month-old DPP6-KO mice compared to WT (Fig. 3D,E, $p < 0.001$). These results indicate that there is a higher accumulation of Aβ in DPP6-KO mice and that this may be important pathologically in AD. Note that, in contrast to humans, normal aging WT mice do not develop Aβ plaques, likely due to differences in the Aβ sequence between rodent and human (Kitazawa, et al., 2012; Dyrks, et al., 1993). We also have never seen the typical Aβ plaques in the aging WT or DPP6-KO mice labeled with the Aβ antibody, nor were any Aβ plaques detected using Bielschowsky staining (data not shown). IF of the NeuN+ large puncta showed some colocalization with small puncta of Aβ (Fig. 3F, as noted in Lin et al., 2020). Sometimes IF for Aβ colocalized substantially with NeuN (right image in Fig. 3F). This overlapping distribution was now confirmed with EM-immunogold of the NeuN+ swellings; Aβ immunogold labeling in some cases colocalized substantially with that of NeuN in swellings (Fig. 3G).

Aβ accumulations in the hippocampus of 12-month-old DPP6-KO mice were associated with microglia (Fig. 4A–C) and astrocytes (Fig. 4D–F). Labeling for Aβ was within the microglial somas and scattered along the Iba1-labeled microglial processes as numerous punctate structures, consistent with the internal location of Aβ in microglia shown by Sos et al. (Sos et al., 2020). These structures probably correspond to the irregular Aβ-labeled puncta and small somas seen in Figure 3A. In contrast to Aβ-labeling associated with glial markers, labeling for Aβ did not associate closely with most apical dendrites labeled for MAP2 (CA1 stratum radiatum; Fig. 4G–I). Little labeling for Aβ was found in the CA1 pyramidal neuron somas and apical dendrites in 12-month-old WT and DPP6-KO mice (Fig. 4G–I) but labeling in apical dendrites was seen occasionally in 8-week-old WT and DPP6-KO mice (Fig. 4J–L). Note also that the MAP2-labeled dendrites appeared more irregular and dysmorphic in the 12-month-old DPP6-KO mice compared to 12-month-old WT mice and 8-week-old WT and DPP6-KO mice. Labeling for Aβ also was found in some interneurons (Fig. 4I–L). Thus, the overall trend in the CA1 region of the hippocampus was a large increase in labeling in small irregular patches in the neuropil of 12-month-old DPP6-KO mice, mainly associated with glia, while there was a decrease in labeling for Aβ in the neuronal somas and apical dendrites in both WT and DPP6-KO mice at 12 months compared to 8 weeks.

## Increased Hyper-phosphorylated tau accompanies neurodegeneration in aged DPP6-KO mice

To determine hyper-phosphorylated tau expression level in aging DPP6-KO mice, we performed western blot analysis of hippocampal tissue total lysate. The results showed that AT8, AT180 and cleaved-tau expression levels are significantly increased in DPP6-KO mice compared to WT (Fig. 5A–B: $p$ <0.01–0.001, n = 6–8 for WT and KO each). Also, in IF staining for AT8 in aged WT and DPP6-KO mice brain sections (Fig. 5C), we found that the intensity of AT8 is higher in the hippocampus of DPP6-KO mice compared to WT (Fig. 5D, $p$ <0.001). In the WT, low labeling was found in some apical dendrites of the stratum radiatum; in contrast, in DPP6-KO mice, the AT8 labeling is not concentrated in the major dendrites as found in the WT but is much more abundant and spread out in an irregular branching pattern; this presumably is due to tau filament formation and the corresponding microtubule dysfunction (Fig. 5C). IF labeling with MAP2 showed an opposite pattern to the AT8, i.e., MAP2 was abundant and distinctive in apical dendrites and associated neuropil of cortex and hippocampus in the aging WT and much reduced in the dendrites in DPP6-KO (Fig. 5E–H). We also found that protein levels of α-synuclein and P19ARF in the DPP6-KO hippocampal tissue lysate were significantly increased compared to WT (Fig. 5I,J, α-synuclein n = 5, $p$<0.05, n = 5; Fig. 5K,L, P19ARF n=5, $p$ <0.0001). α-synuclein accumulation is linked to several neurodegenerative diseases including Parkinson's disease, dementia with Lewy bodies, and multiple system atrophy (Bernal-Conde et al., 2020), and P19ARF is a marker of aging and cellular senescence (Cheng et al., 2017; Wagner and Wagner, 2022). These results suggest that DPP6 helps to stabilize neuronal structure/function. Accordingly, we found previously (Lin et al., 2013, 2018) that there are fewer synapses in adult DPP6-KO mice (8 weeks old) and these are less functional compared to WT. It may be that in the aging mice (12 months), lack of DPP6 further destabilizes dysfunctional synapses in the aging brain, leading to an aberrant increase in tau phosphorylation and neuronal injury.

## Aging DPP6-KO mice show enhanced neuroinflammation

Given that neuroinflammation is associated with AD and other neurodegenerative disorders, we examined neuroinflammation in aging DPP6-KO mice. We first measured the expression levels of astrocytes and microglia in brain sections, and then measured the levels of proinflammatory or anti-inflammatory cytokines in the blood serum of aged DPP6 KO mice. Figure 6A–C shows the IF staining for GFAP in astrocytes in 12-month WT and DPP6-KO mice brains. There was higher labeling for GFAP in DPP6-KO mice in whole brain (Fig. 6A) and in the hippocampus (Fig. 6B). Astrocytes were increased in size and number compared to WT (Fig. 6C, $p$ <0.0001 in size and $p$ <0.05 in number). Figure 6D,E shows the IF staining of Iba1 for microglia in hippocampus (Fig. 6D), with enlarged microglia and higher intensity in DPP6-KO mice compared to WT in brain and hippocampus (Fig. 6E, $p$ <0.01). Microglia were increased in size and number compared to WT (Fig. 6E, $p$ <0.0001 in both size and number). We also performed IF staining in sections from 8-week WT and DPP6-KO mice to determine whether there was inflammation in younger adults. We found that there were no significant differences in the intensities of either GFAP or Iba1 in 8-week WT and DPP6-KO brain sections ($p$ >0.05 for either GFAP or Iba1, data not shown).

We also found GFAP+ astrocyte processes (Fig. 6F) and Iba1+ microglial processes (Fig. 6G) surrounding the newly described NeuN+ swellings. Astrocyte processes often formed ring-like structures directly contiguous with the outer border of some of the NeuN+ structures (Fig. 6F). Astrocytes seem to make more intimate and prevalent contacts with the novel NeuN+ puncta than microglia; this may reflect distinctive roles played by astrocytes versus microglia in clearing Aβ and other degeneration-associated material (Mulder et al., 2014).

Next, we detected inflammation by measuring the proinflammatory or anti-inflammatory cytokines in mouse blood serum with Cytokine Array / Chemokine Array. We found that the levels of IL-1, IL-2, IL-6, MCP-1(Monocyte chemotactic protein 1), and MIP-1β (Macrophage inflammatory protein-1β, known as CCL4) were significantly increased in DPP6-KO mice compared to WT (Fig. 6H–L) (Griffin et al., 1989; Eriksson et al., 2011; Brosseron et al., 2014; Bauer et al., 1991; Verite et al., 2017; Zhu et al., 2014), but not in 8-week adults (data not shown). Increases in some cytokines have been described also in humans with AD (Brosseron et al., 2014; Zheng et al., 2016). These results indicate that aging DPP6-KO mice show neuroinflammation that may be involved in the pathogenesis of neuronal injury and death leading to progressive dementia.

## Similar novel NeuN+ labeled structures are found in hippocampal CA1 of AD donors

As in aging mice, labeling for NeuN in the CA1 of the human hippocampus (Fig. 7) was prominent in some pyramidal neuron somas and apical dendrites in brains from both control and AD donors. There also were some NeuN+, irregular remains of more degenerate neurons seen in the AD brains (Fig. 7D,K); and DAPI labeling revealed some unusual clusters of cells (Fig. 7E). We looked for the novel NeuN+ structures that we had found in the aging mice CA1; the pattern was not clear, but we did find some clusters that appear to represent similar NeuN+ structures in both control (Fig. 7F,H) and AD (Fig. 7G,I) human brains. These structures had partial to full colocalization with synaptophysin, suggesting that they represent the same kind of clusters (Fig. 7H,I) as noted in mice. The NeuN+ clusters of puncta appeared to be a little more common overall in the AD compared to the control human brains, but numbers were too small to quantify and they were notably less common than the clusters seen in aging mice in our studies (Lin et al. 2020 and this study). Also, as described for the aging mice, Aβ was seen in some accumulations that overlapped partly with some NeuN labeling; in the human, these overlaps are seen in Aβ plaques (Fig. 7J). MAP2 labeling in these donors was not as prominent in pyramidal neuron apical dendrites (Fig. 7K,L) as that seen in aging mice and had a more scattered and irregular distribution. Examples also were seen of labeling with DAPI+NeuN+MAP2 in a small cluster of irregular somas and cell processes (Fig. 7K) and colocalization of MAP2 with NeuN in the NeuN+ clusters of puncta (Fig. 7L) as described in aging mice (Lin et al., 2020).

## Aging DPP6-KO mice have circadian rhythm disruption as determined by home-cage locomotor activity

Since the structural and IF labelling data suggested enhanced neurodegeneration in aging DPP6-KO mice, we used a common behavioral assay indicative of progressive neurodegeneration, analysis of circadian rhythms (Lin et al., 2018). This disruption has

been associated with many of the indicators of AD, such as increased Aβ, tau pathologies, and neuroinflammation (Homolak et al., 2018; Hoogendijk et al., 1996; Weldemichael et al., 2010), similar to what we have described here in the hippocampus and overall in the brain of aging DPP6-KO mice. These disruptions in circadian rhythms in patients with AD involve a reduction in scale invariance of activity patterns, with a disruption in the rest-activity cycle. There typically is a disruption of normal sleep patterns, i.e., patients are more active at night and sleep is fragmented with frequent awakenings. There is a reduction in total melatonin and loss of its normal secretion rhythm. And there can be alterations in periodic changes in core body temperature (Videnovic et al., 2014, Musiek and Holtzman, 2016, Uddin et al., 2020). While pathological disruption of circadian rhythms likely involves pathologies of control centers in the hypothalamus, direct disruption of clock mechanisms within the hippocampus itself also have been implicated (Videnovic et al., 2014).

We have previously published a study on locomotor activity in 8-week old DPP6-KO using the home cage test; we found that locomotor activity was not significantly different between WT and DPP6-KO mice either in light-on or light-off conditions (Lin et al., 2018). In contrast, the current results showed that 12-month DPP6-KO mice have increased locomotor activity compared to WT mice in Ambulation and Fine movements (Fig. 8A; Two-way ANOVA, $p < 0.05$ and $p < 0.01$) but not in Rear movement (Fig. 8A; Two-way ANOVA, $p > 0.05$) during the light-on phase. There was no significant increase during the light-off phase for all three movements (Fig. 8A; Two-way ANOVA, $p > 0.05$). When light-on and light-off times were pooled, the activities from Fine movement of DPP6-KO mice were still significantly increased compared to WT groups (Fig. 8B, Student's t-test, $p < 0.05$), but no differences in Ambulation movement and Rear movement were seen (Fig. 8B; Student's t-test, $p > 0.05$).

We then compared the hourly activities at the same time of light-on and light-off in the three movements (Fig. 8C). KO mice showed hyperactivity relative to WT throughout much of the light period (beginning and end) and the middle of the dark period but showed less activity during times when it peaked in WT mice at the start and end of the dark period. The latter is expected in WT mice, since mice are nocturnal, showing greater activity at night than in the day (Refinetti 2004; Angelakos et al., 2017). Thus, the normal circadian rhythm pattern of mice appears to be disrupted in the DPP6-KO. Especially, there are periods of abnormally high activity during the day and middle of the night that may be similar to increased wake periods in disruption of the rest-activity cycle/circadian rhythms in humans with AD (Nagele et al., 2003; Weldemichael and Grossberg, 2010; Vijayakumar and Vijayakumar, 2013; Zhou et al., 1998). It is also interesting that the mouse model of AD, 5xFAD, exhibits hyperactivity (Oblak et al., 2021). This hyperactivity might explain the lower body weight in DPP6-KO mice despite normal feeding behavior. Significant hyperactivity also was seen in 8-week DPP6-KO mice with open field test (although not with home-cage locomotor activity) and they also showed lower body weight despite normal feeding behavior at that age (Lin et al., 2018). Lower body weight could also be related to a possible link between DPP6 and diabetes (Dusaulcy et al., 2019), and DPP6 may have other yet unknown effects on metabolism. While specific effects on circadian rhythms would be expected to be different between the normally nocturnal mice and diurnal human,

these findings of general rest-activity disruption suggest that aging DPP6-KO mice exhibit behavioral changes that have been linked to AD.

## DISCUSSION

Here we found evidence that aging DPP6-KO mice show changes related to AD/dementia; specifically, based on the current work in conjunction with our previous studies, DPP6-KO mice approximate and enhance AD-associated pathology over an aging time course. The new findings of the current study include the following. Aging DPP6-KO brains and hippocampi were reduced in size, as shown with *in vivo* MRI, and as noted in dementia (Vijayakumar and Vijayakumar, 2013). DPP6-KO hippocampi contained smaller and fewer neurons with less NeuN labeling, and had diagnostic biomarkers of AD present in the associated neuropil, including accumulation of Aβ and increase in expression of hyper-phosphorylated tau (Homolak et al., 2018; Jones et al., 2013). Changes studied at synapses include increased APP and presynaptic invaginations. Astrocytes and microglia increased in size and number and showed close associations with Aβ in the aging DPP6-KO mice as known for AD (Osborn et al., 2016; Ries and Sastre, 2016; Spanic et al., 2019). Levels of proinflammatory or anti-inflammatory cytokines increased also in aging DPP6-KO mice as shown for AD (Brosseron et al., 2014; Osborn et al., 2016; Zheng et al., 2016; Spanic et al., 2019). We also showed that aging DPP6-KO mice display circadian dysfunction, a common symptom of AD (Musiek et al., 2015). As discussed in the Introduction, DPP6 already has been linked to dementia in several studies (Rademakers et al., 2005; Zelaya et al., 2015; Cacace et al., 2019). Thus, our study supports a role of the mutation or loss of DPP6 in at least some forms of dementia.

The substantial increases in size and number of astroglial and microglial processes that we describe here in the aging DPP6-KO mice are consistent with findings for AD/dementia, in which both astrocytes and microglia increase in activation and number and are attracted to accumulations of amyloid plaques and fibrils and dystrophic neurons (Osborn et al., 2016; Ries and Sastre, 2016; Spanic et al., 2019). This is consistent with astroglial ingestion of Aβ and associated degenerate material (Nagele et al., 2003; Jones et al., 2013). Glia can ingest and remove degeneration debris, although dysregulation of the glia may lead to increased, abnormal accumulations of this material. In particular, activation of microglia may change with development (Floden and Combs, 2011) and depends also on the state of the amyloid, i.e., monomers vs. protofibrils vs. fibrils, with protofibrils producing the greatest stimulation of microglia (Paranjape et al., 2012).

Here we also provide new data on the novel clusters of large, NeuN+ puncta that we described previously (Lin et al., 2020). These structures appear in 3-month old DPP6-KO mice (but not WT) and are better developed in 12-month old KO mice compared to WT. We had shown then that these structures could be identified with NeuN labeling and fully colocalized with synaptophysin and chromogranin A; they also partially labeled for MAP2, Aβ, APP, α-synuclein, and phospho-tau, and with synapsin-1 and VGluT1 labeling on their periphery. We confirmed in that study that most of these structures are aberrant, swollen presynaptic terminals, utilizing EM including immunogold labeling. Here now we combined IF with EM-immunogold labeling to confirm that both APP and Aβ are prevalent in these

structures; and we showed with immunofluorescence the presence of similar structures in aging humans with AD as well as in the control human brains. The presence of some of these novel clusters of NeuN+ puncta in the human donors was expected because possible corresponding, aberrant swollen presynaptic terminals have been mentioned by others (Terry et al., 1963; Zhou et al., 1998), as discussed in Lin et al. (2020). These new data thus reaffirm our contention that these novel structures are a typical structure in the aging brain and that they are enhanced in dementia, at least when associated with the loss of DPP6. The apparent abundance of these novel structures in aging mice, both in WT and to a greater extent in the DPP6-KO (Lin et al., 2020 and this study), compared to humans might indicate that they play a greater role in neurodegenerative diseases such as dementia in the aging mouse brain.

### Differences in Aβ and phospho-tau between WT and DPP6-KO resemble differences described with aging in hippocampal CA1

There were distinctive and opposite changes in labeling for NeuN and MAP2 versus Aβ and the phospho-tau protein, AT8, in the CA1 region of the hippocampus, between the aging WT and DPP6-KO mice. Thus, labeling in the pyramidal neuron somas and apical dendrites for NeuN and MAP2 was strong in the 12-month-old WT and notably lower in the DPP6-KO; and the labeling pattern indicates a reduction in size and number of these structures in the KO. In a dramatically opposite pattern, Aβ and AT8 labeling in the 12-month-old mice revealed relatively few, weakly-labeled somas and apical dendrites within the stratum radiatum in the WT and showed strong labeling of irregular puncta throughout this area in the KO. This pattern is consistent with the model for progressive degeneration of the CA1 apical dendrites in aging as may occur with AD, described by Takahashi et al. (Takahashi et al., 2013). Thus, the apical dendrites initially are robust and have abundant MAP2 and only traces of Aβ and phospho-tau. Then, as aging progresses, MAP2 in these dendrites is reduced and Aβ and phospho-tau also accumulate, forming irregular structures derived partly from the degeneration of the apical dendrites. In AD, Aβ oligomers may accumulate both intra- and extracellularly in/around the dendrites and spine synapses, and have direct effects on synapse function, while the abnormally phosphorylated tau migrates from axons to the somas, dendrites and spines, also affecting synaptic function (Forner et al., 2017, 2019; Mijalkov et al., 2021). These data suggest that KO of DPP6 may result in similar changes in the CA1 as found in the degeneration accompanying AD or related forms of dementia. Note however, that the small, irregular puncta seen with Aβ and AT8-phospho tau labeling in the 12-month DPP6-KO are widespread throughout the radiatum, and do not form into large plaque deposits as seen in the CA1 of a 10-month-old 5xFAD AD model mouse (Lin et al., 2020). This could mean that the differences between WT and DPP6-KO at 12 months is comparable to early and middle stages in development of AD/dementia, but it more likely reflects distinct differences in aging/neurodegeneration in mice versus humans. With the current evidence, and lack of senile Aß plaques found in these mice, it can be said at best that DPP6-KO mice approximate and enhance AD-associated pathology over an aging time course.

These findings also are consistent with earlier studies of DPP6-KO mice, where DPP6 mutants show negative effects on neuronal and synaptic development and function and mice

show behavioral/learning deficits (Lin et al., 2013, 2014, 2018). For example, EM studies revealed that synaptic spines and their postsynaptic densities in the CA1 stratum radiatum are smaller in the young adult DPP6-KO mice compared to WT (Lin et al., 2018). And brain weight in these mice is significantly lower in the KO versus WT at both 3 and 6 months old (but not at P0) (Lin et al., 2018). Overall, this suggests that loss of DPP6 can cause learning deficits via direct functional defects in the hippocampus that start early in adult life and eventually lead to enhancement of neurodegenerative diseases such as dementia in old age.

### DPP6 supports normal synaptic function and suppresses neurodegeneration

As we have noted, DPP6 regulates dendrite excitability in the CA1 hippocampus because it functions as an auxiliary unit to Kv4.2 potassium channels of synapses; its absence has profound effects on the expression and responsiveness of A-type potassium channel currents (Sun et al., 2011). While most functional studies of Kv4.2 concentrate on the postsynaptic molecules, this channel also is found in the presynaptic terminal and is trafficked there along the axon (Bellotti et al., 2021). DPP6 may also affect neuronal function independent of Kv4.2; it interacts with filopodial myosin and extracellular fibronectin (Lin et al., 2013), and it also binds to Kv4.3 (Ma et al., 2022), which has a different normal distribution pattern compared to Kv4.2 (Serôdio et al., 1998; Burkhalter et al., 2006). Two-month-old mice lacking DPP6 show altered synaptic structure and function, and impairment of recognition, learning and memory (Lin et al., 2018). Twelve month-old mice show increases in numbers and prevalence of novel NeuN-positive structures in the hippocampal CA1 that contain neurodegenerative proteins such as amyloid beta and phospho-tau; these structures are aberrant swollen presynaptic terminals in this region, which also shows other signs of increased neurodegeneration (Lin et al., 2018). Now in the present study, we provide more definitive data on the changes in this region of 12-month-old mice lacking DPP6, including reduction of hippocampal volume, increased apoptosis, increases in amyloid beta and phospho-tau deposits, increased APP in synapses and associated increases in synaptic invaginations, as well as disrupted circadian rhythm. We have not yet studied other behavioral changes in the 12-month-old DPP6-KO, but we expect that learning and memory deficits are at least as bad and likely worse than those seen in the 2-month-old KO. Thus, these series of studies have established that DPP6 is important to supporting normal potassium channel function at synapses and its absence leads to several different synaptic abnormalities and signs of neurodegeneration throughout this region of the hippocampus; and this is linked to significant problems in learning and memory.

Direct changes detected in synapses in mice lacking DPP6 include increased APP in synapses and associated increases in synaptic invaginations. While changes in the presynaptic membrane with increased APP have not been studied in rodents, a number of other changes in synapses have been reported (Lee et al., 2010; Wang et al., 2012). Overexpression of APP generally causes increases in mammalian spine synapses, although there is a decrease in both cerebral cortex and CA1 in 12-month old APP-overexpressing mice (Lee et al., 2010), similar to the findings for the DPP6 mutant described here. Also, 18-month-old mutant mice that express a modified APP show increased surface area of inhibitory axo-axonic terminals on CA1 pyramidal neuron-axon initial segments (Sos et al.,

2020). Interestingly, in *Drosophila*, there is a dramatic increase in the presynaptic membrane in neuromuscular junctions via budding when an APP homolog is overexpressed (Torroja et al., 1999). A similar budding of the presynaptic membrane would explain the increase in intertwining invaginations of adjacent terminals in the DPP6 mutant mouse as described here. It is not known if the increased invaginations would adversely affect the synaptic function, but given the involvement of invaginations in synapse function and plasticity, we would expect that the dynamics of synapse function would be altered (Petralia et al., 2015, 2018, 2021).

But does loss of DPP6 play a direct role in the development of AD and related forms of dementia? As we have noted in the Introduction, there is good genetic evidence of an association of DPP6 and AD (Cacace et al., 2019; Rademakers et al., 2005). However, no link was found between DPP6 and AD in a European American population (Kirola et al., 2021); but these authors (Kirola et al., 2021) do point out the limitations of their study in light of the findings of Cacace et al. (Cacace et al., 2019, 2021) including the latter's identification of carriers of missense variants in some patients, alterations in protein structure by missense mutations, and presence of some intronic structural variants (Kirola et al. only examined exonic regions). Another factor that complicates interpretations of our findings in DPP6-KO mice in relation to AD is the differences in manifestation of neurodegenerative diseases in the mice versus human, i.e., DPP6-KO mice have more abundant NeuN+-swellings, but these swellings are uncommon in human AD, and mice apparently lack the amyloid beta plaques found in humans. However, we also found previously that the NeuN+swellings are more abundant in the AD/plaque-containing mouse model compared to WT (Lin et al., 2020).

The key to the connection between DPP6 and its associated potassium channels and AD is likely in the synapse. There is an enormous body of literature linking potassium channels with AD (Villa et al., 2020). For example, amyloid beta can modulate various kinds of potassium channels in the hippocampus (Mayordomo-Cava et al., 2015). APP is prevalent in presynaptic terminals (Laßek et al., 2013; Weingarten et al., 2017), and as shown here, increases in the DPP6-KO. Also, small quantities of amyloid beta in the normal brain may help to mediate synaptic plasticity of learning and memory, and amyloid beta may only become pathological when homeostatic control in the synapse is disrupted (Puzzo et al., 2012; Parihar and Brewer, 2010; Lee et al., 2014; Ricciarelli et al., 2014). But perhaps the most direct link between DPP6 and AD is through cellular prion proteins, which are prevalent in the normal brain, and are found at hippocampal synapses (Godsave et al., 2015). Cellular prion proteins act as amyloid beta-oligomer receptors, and are mediators of synaptic dysfunction via amyloid beta-oligomers (Laurén et al., 2009; Um and Strittmatter, 2013). And similar to prion proteins, propagation and aggregation of amyloid beta, as well as phospho-tau and α-synuclein, may proceed via a seeding/nucleation, prion-like mechanism (Soto et al., 2018; Zhang et al., 2021), perhaps instigated by the initial small molecular disruptions of homeostasis at the synapse.

Most interestingly, DPP6 is a prion protein interactor, and modulation of Kv4.2 potassium channels by prion proteins is mediated by DPP6 (Mercer et al., 2013). But lack of DPP6 may also affect synapses independent of potassium channels through interactions with

filopodial myosins and extracellular fibronectin, affecting synapse and filopodia formation (Lin et al., 2013). In some cases, fibronectin can induce amyloid beta deposition (Howe et al., 2018; Maas et al., 2008), so perhaps lack of DPP6 disrupts fibronectin organization in the local synaptic environment, and this affects amyloid deposition. Also, at least one type of myosin is involved in processing of APP/amyloid beta (Argellati et al., 2009). The direct link between abnormal amyloid beta aggregation associated with synapses and accumulation of phospho-tau is not clear, but a number of studies support phospho-tau induction via amyloid beta (Forner et al., 2017), and evidence suggests that the amyloid beta aggregation at synapses induces this tauopathy (Wu et al., 2018); again this neurodegeneration pattern of AD and other diseases may all depend on homeostasis at the synapse (Forner et al., 2017, 2019; Mijalkov et al., 2021; Parihar and Brewer, 2010). So, it is possible that abnormal synaptic structure/function due to the absence of DPP6, and perhaps including potassium channel dysfunction and also the dis-regulation of prion proteins, promotes the formation/accumulation of amyloid beta and other changes that can lead to neurodegenerative diseases such as AD.

The complexity of associations of DPP6 with other proteins, especially at synapses, makes it difficult to isolate specific roles that DPP6 plays in AD. The molecular complex of DPP6 and Kv4.2 likely includes other dipeptidyl aminopeptidase-like proteins such as DPP10, as well as $K^+$ channel interacting proteins (KChIPs) (Kitazawa et al., 2015). Within these complexes, DPP6 and DPP10 may form heterodimers, based on high structural identity and *in vitro* studies (Ren et al., 2005; Bezerra et al., 2015; Kitazawa et al., 2015). Notably, like DPP6, DPP10 is associated with AD and other neurodegenerative diseases (McNicholas et al., 2009; Chen et al., 2014) and is found in hippocampal neurons (Wang et al., 2014). Future studies will determine if DPP10 is affected in the DPP6-KO; if it is a common associate in a complex with DPP6 and Kv4.2, then the loss of DPP6 could affect the levels of DPP10 and perhaps adversely affect the function of the potassium channel complexes and lead directly to some of the changes that we see in the DPP6-KO.

## Limitations of the study and future directions

There are some specific limitations of this research that we hope to resolve in future studies. First, we were not able to determine the localization and associations of DPP6 in specific structures in the brains of aging mice; we need to obtain or develop DPP6 antibodies that work well for IF. We were not able to identify changes in DPP6 and associated proteins in the human donors with AD. For this we will need to obtain frozen, unfixed human donor tissues to study the role of DPP6 in AD using immunoblots and coIPs. We also have not looked at aging in related KOs, such as Kv4.2 and DPP10-KO mice.

In addition, the value of any gene loss studies may be compromised by the use of traditional/global/full KO models (Teng et al., 2013; El-Brolosy and Stainier, 2017). Such deletions will likely affect an animal in development, including embryonic, immature, young adult, as well as in aging. Developing successful KOs to study aging is difficult, as they often result in embryonic lethality or other problems in early development. A common problem with full KO models is the compensation of a deleted protein by related proteins (El-Brolosy and Stainier, 2017), such as we discussed above for possible dimers of DPP6 and DPP10.

Some of these problems may be averted by developing alternative methods such as gene knockdown, or a conditional KO model that targets selected tissues or particular times in development (El-Brolosy and Stainier, 2017; Pons et al., 2021).

Current work in our lab on the role of DPP6 in aging and AD includes continuing studies of the brains of human donors with AD, more *in vivo* studies such as EEG to study sleep disorders and seizures in the aging KO mice, *in vivo* injection of AAV-DPP6 to study rescue of its function including behavioral changes. In addition, our study has identified novel NeuN+ structures in aging mice, and we want to determine if these structures are native biomarkers of aging and dementia in mice instead of the Aβ plaques seen in human conditions. How do these structures form during development? How can their formation be inhibited, and the aging brain rescued from their effects?

In conclusion, the current study continues the extensive work of this laboratory to discern the nature of DPP6 function in the brain. Now that we have provided compelling evidence of a role of DPP6 in AD and other neurodegenerative disorders, we will continue to explore the function of DPP6 and its associated proteins in greater depth, during development and into old age, in mice and in humans. Hopefully, this research on the relation of DPP6 with AD will yield data that impact on clinical studies leading to treatments of AD and other neurodegenerative disorders.

## ACKNOWLEDGMENTS

This work was supported by the Intramural Research Program of the *Eunice Kennedy Shriver* National Institute of Child Health and Human Development. R.S. Petralia and Y.-X. Wang were supported by the Intramural Research Program of NIH/National Institute on Deafness and Other Communication Disorders (NIDCD) (Advanced Imaging Core-ZIC DC000081). We thank Dr. Hoffman's lab members, Yujun Hou (NCI), and Rose Marie Karlsson (NIMH) for helpful suggestions. We also thank the NIH Mouse Imaging Facility and the NICHD Microscopy and Imaging core including Dr. Vincent Schram and Ling Yi for technical assistance. We thank Dr. Olivia Spicer from the NIH NeuroBioBank and Dr. Sabina Berretta from the Harvard Brain Tissue Resource Center for providing the human tissues; and we deeply appreciate the tissue contributions from all the donors.

## REFERENCES

Angelakos CC, Watson AJ, O'Brien WT, Krainock KS, Nickl-Jockschat T, Abel T (2017) Hyperactivity and male-specific sleep deficits in the 16p11.2 deletion mouse model of autism. Autism research : official journal of the International Society for Autism Research 10:572–584. doi:10.1002/aur.1707 [PubMed: 27739237]

Argellati F, Domenicotti C, Passalacqua M, Janda E, Melloni E, Marinari UM, Pronzato MA, Ricciarelli R (2009) Protein kinase C-dependent alpha-secretory processing of the amyloid precursor protein is mediated by phosphorylation of myosin II-B. FASEB J 23:1246–1251. doi:10.1096/fj.08-119263 [PubMed: 19103644]

Bauer J, Strauss S, Schreiter-Gasser U, Ganter U, Schlegel P, Witt I, Yolk B, Berger M (1991) Interleukin-6 and alpha-2-macroglobulin indicate an acute-phase state in Alzheimer's disease cortices. FEBS letters 285:111–114. doi:10.1016/0014-5793(91)80737-n [PubMed: 1712317]

Bellotti A, Murphy J, Lin L, Petralia R, Wang YX, Hoffman D, O'Leary T (2021) Paradoxical relationships between active transport and global protein distributions in neurons. Biophys J 120:2085–2101. doi:10.1016/j.bpj.2021.02.048 [PubMed: 33812847]

Bernal-Conde LD, Ramos-Acevedo R, Reyes-Hernández MA, Balbuena-Olvera AJ, Morales-Moreno ID, Argüero-Sánchez R, Schüle B, Guerra-Crespo M (2020) Alpha-Synuclein Physiology and Pathology: A Perspective on Cellular Structures and Organelles. Front. Neurosci, 13: 1399–1421. 10.3389/fnins.2019.01399 [PubMed: 32038126]

Bezerra GA, Dobrovetsky E, Seitova A, Fedosyuk S, Dhe-Paganon S, Gruber K (2015) Structure of human dipeptidyl peptidase 10 (DPPY): a modulator of neuronal Kv4 channels. Sci Rep 5;5:8769. doi: 10.1038/srep08769 [PubMed: 25740212]

Bock I, Nemeth K, Pentelenyi K, Balicza P, Balazs A, Molnar MJ, Roman V, Nagy J, Levay G, Kobolak J, Dinnyes A (2016) Targeted next generation sequencing of a panel of autism-related genes identifies an EHMT1 mutation in a Kleefstra syndrome patient with autism and normal intellectual performance. Gene 595:131–141 [PubMed: 27651234]

Brosseron F, Krauthausen M, Kummer M, Heneka MT (2014) Body fluid cytokine levels in mild cognitive impairment and Alzheimer's disease: a comparative overview. Mol Neurobiol 50:534–544. doi:10.1007/s12035-014-8657-1 [PubMed: 24567119]

Burkhalter A, Gonchar Y, Mellor RL, Nerbonne JM (2006) Differential expression of I(A) channel subunits Kv4.2 and Kv4.3 in mouse visual cortical neurons and synapses. J Neurosci 26:12274–12282. doi:10.1523/jneurosci.2599-06 [PubMed: 17122053]

Cacace R, Heeman B, Van Mossevelde S, De Roeck A, Hoogmartens J, De Rijk P, Gossye H, De Vos K, De Coster W, Strazisar M, De Baets G, Schymkowitz J, Rousseau F, Geerts N, De Pooter T, Peeters K, Sieben A, Martin JJ, Engelborghs S, Salmon E, Santens P, Vandenberghe R, Cras P, DD PP, vS JC, vD CM, van der Zee J, Sleegers K, Van Broeckhoven C, Consortium B (2019) Loss of DPP6 in neurodegenerative dementia: a genetic player in the dysfunction of neuronal excitability. Acta Neuropathol 137:901–918. doi:10.1007/s00401-019-01976-3 [PubMed: 30874922]

Cacace R, Van Broeckhoven C (2021) Reply: Lack of evidence supporting a role for DPP6 sequence variants in Alzheimer's disease in the European American population. Acta Neuropathol 141:625–626. doi:10.1007/s00401-021-02277-4 [PubMed: 33591373]

Caselli RJ, Beach TG, Knopman DS, Graff-Radford NR (2017) Alzheimer Disease: Scientific Breakthroughs and Translational Challenges. Mayo Clinic proceedings 92:978–994. doi:10.1016/j.mayocp.2017.02.011 [PubMed: 28578785]

Chen T; Gai WP; Abbott CA (2014) Dipeptidyl peptidase 10 (DPP10): A voltage gated potassium channel associated protein is abnormally expressed in Alzheimer's and other neurodegenerative diseases. Biomed Res Int 209398. doi: 10.1155/2014/209398

Cheng Z, Zheng YZ, Li YQ, Wong CS (2017) Cellular Senescence in Mouse Hippocampus After Irradiation and the Role of p53 and p21. J Neuropathol Exp Neurol 1;76(4):260–269. doi: 10.1093/jnen/nlx006. [PubMed: 28340115]

Den HT, van der Lijn F, Koudstaal PJ, Hofman A, van der Lugt A, Krestin GP, Niessen WJ, Breteler MM (2010) A 10-year follow-up of hippocampal volume on magnetic resonance imaging in early dementia and cognitive decline. Brain: a journal of neurology 133:1163–1172. doi:10.1093/brain/awq048 [PubMed: 20375138]

DeTure MA, Dickson DW (2019) The neuropathological diagnosis of Alzheimer's disease. Mol Neurodegener 14:32. doi:10.1186/s13024-019-0333-5 [PubMed: 31375134]

Dyrks T, Dyrksb E, Maste CL and Beyreutherb K (1993) Amyloidogenicity of rodent and human PA4 sequences. Federation of European Biochemical Societies 324 (2):231–236

Egger G, Roetzer KM, Noor A, Lionel AC, Mahmood H, Schwarzbraun T, Boright O, Mikhailov A, Marshall CR, Windpassinger C, Petek E, Scherer SW, Kaschnitz W, Vincent JB (2014) Identification of risk genes for autism spectrum disorder through copy number variation analysis in Austrian families. Neurogenetics 15:117–127 [PubMed: 24643514]

El-Brolosy MA, Stainier DYR (2017) Genetic compensation: A phenomenon in search of mechanisms 13;13(7):e1006780. doi: 10.1371/journal.pgen.1006780

Eriksson UK, Pedersen NL, Reynolds CA, Hong MG, Prince JA, Gatz M, Dickman PW, Bennet AM (2011) Associations of gene sequence variation and serum levels of C-reactive protein and interleukin-6 with Alzheimer's disease and dementia. Journal of Alzheimer's disease : JAD 23:361–369. doi:10.3233/jad-2010-101671 [PubMed: 21116047]

Floden AM, Combs CK (2011) Microglia demonstrate age-dependent interaction with amyloid-β fibrils. Journal of Alzheimer's disease: JAD 25:279–293. doi:10.3233/jad-2011-101014 [PubMed: 21403390]

Forner S, Baglietto-Vargas D, Martini AC, Trujillo-Estrada L, LaFerla FM (2017) Synaptic Impairment in Alzheimer's Disease: A Dysregulated Symphony. Trends Neurosci 40:347–357. doi:10.1016/j.tins.2017.04.002 [PubMed: 28494972]

Forner S, Martini AC, Prieto GA, Dang CT, Rodriguez-Ortiz CJ, Reyes-Ruiz JM, Trujillo-Estrada L, da Cunha C, Andrews EJ, Phan J, Vu Ha J, Chang A, Levites Y, Cruz PE, Ager R, Medeiros R, Kitazawa M, Glabe CG, Cotman CW, Golde T, Baglietto-Vargas D, LaFerla FM (2019) Intra- and extracellular β-amyloid overexpression via adeno-associated virus-mediated gene transfer impairs memory and synaptic plasticity in the hippocampus. Sci Rep 9:15936. doi:10.1038/s41598-019-52324-0 [PubMed: 31685865]

Godsave SF, Peters PJ, Wille H (2015) Subcellular distribution of the prion protein in sickness and in health. Virus research 207:136–145. doi:10.1016/j.virusres.2015.02.004 [PubMed: 25683509]

Gouras GK, Tsai J, Naslund J, Vincent B, Edgar M, Checler F, Greenfield JP, Haroutunian V, Buxbaum JD, Xu H, Greengard P, Relkin NR (2000) Intraneuronal Abeta42 accumulation in human brain. Am J Pathol 156:15–20. doi:10.1016/s0002-9440(10)64700-1 [PubMed: 10623648]

Griffin WS, Stanley LC, Ling C, White L, MacLeod V, Perrot LJ, White CL 3rd, Araoz C (1989) Brain interleukin 1 and S-100 immunoreactivity are elevated in Down syndrome and Alzheimer disease. Proc Natl Acad Sci U S A 86:7611–7615. doi:10.1073/pnas.86.19.7611 [PubMed: 2529544]

Gyure KA, Durham R, Stewart WF, Smialek JE, Troncoso JC (2001) Intraneuronal abeta-amyloid precedes development of amyloid plaques in Down syndrome. Archives of pathology & laboratory medicine 125:489–492. doi:10.1043/0003-9985(2001)125<0489:iaapdo>2.0.co;2 [PubMed: 11260621]

Han W, Li J, Pelkey KA, Pandey S, Chen X, Wang YX, Wu K, Ge L, Li T, Castellano D, Liu C, Wu LG, Petralia RS, Lynch JW, McBain CJ, Lu W (2019) Shisa7 is a GABA(A) receptor auxiliary subunit controlling benzodiazepine actions. Science 366:246–250. doi:10.1126/science.aax5719 [PubMed: 31601770]

Hernandez-Segura A, Nehme J, Demaria M (2018) Hallmarks of Cellular Senescence. Trends in Cell Biology 28 (6):436–453. 10.1016/j.tcb.2018.02.001 [PubMed: 29477613]

Hoffman DA, Magee JC, Colbert CM, Johnston D (1997) K+ channel regulation of signal propagation in dendrites of hippocampal pyramidal neurons. Nature 387:869–875. doi:10.1038/43119 [PubMed: 9202119]

Homolak J, Mudrovčić M, Vukić B, Toljan K (2018) Circadian Rhythm and Alzheimer's Disease. Medical sciences (Basel, Switzerland) 6. doi:10.3390/medsci6030052

Hoogendijk WJ, van Someren EJ, Mirmiran M, Hofman MA, Lucassen PJ, Zhou JN, Swaab DF (1996) Circadian rhythm-related behavioral disturbances and structural hypothalamic changes in Alzheimer's disease. International psychogeriatrics 8 Suppl 3:245–252; discussion 269–272. doi:10.1017/s1041610297003426 [PubMed: 9154571]

Howe MD, Atadja LA, Furr JW, Maniskas ME, Zhu L, McCullough LD, Urayama A (2018) Fibronectin induces the perivascular deposition of cerebrospinal fluid-derived amyloid-β in aging and after stroke. Neurobiol Aging 72:1–13. doi:10.1016/j.neurobiolaging.2018.07.019 [PubMed: 30172921]

Jack CR Jr., Knopman DS, Weigand SD, Wiste HJ, Vemuri P, Lowe V, Kantarci K, Gunter JL, Senjem ML, Ivnik RJ, Roberts RO, Rocca WA, Boeve BF, Petersen RC (2012) An operational approach to National Institute on Aging-Alzheimer's Association criteria for preclinical Alzheimer disease. Ann Neurol 71:765–775. doi:10.1002/ana.22628 [PubMed: 22488240]

Jones RS, Minogue AM, Connor TJ, Lynch MA (2013) Amyloid-β-induced astrocytic phagocytosis is mediated by CD36, CD47 and RAGE. Journal of neuroimmune pharmacology : the official journal of the Society on NeuroImmune Pharmacology 8:301–311. doi:10.1007/s11481-012-9427-3 [PubMed: 23238794]

Jordà-Siquier T, Petrel M, Kouskoff V, Smailovic U, Cordelières F, Frykman S, Müller U, Mulle C, Barthet G (2022) APP accumulates with presynaptic proteins around amyloid plaques: A role for presynaptic mechanisms in Alzheimer's disease? Alzheimers Dement doi:10.1002/alz.12546

Kirola L, Budde JP, Wang F, Norton J, Morris JC, Cruchaga C, Fernández MV (2021) Lack of evidence supporting a role for DPP6 sequence variants in Alzheimer's disease in the European American population. Acta Neuropathol 141:623–624. doi:10.1007/s00401-021-02271 [PubMed: 33591372]

Kitazawa M, Medeiros R, Laferla FM (2012) Transgenic mouse models of Alzheimer disease: developing a better model as a tool for therapeutic interventions. Current pharmaceutical design 18:1131–1147. doi:10.2174/138161212799315786 [PubMed: 22288400]

Kitazawa M, Kubo Y, Nakajo K (2015) Kv4.2 and accessory dipeptidyl peptidase-like protein 10 (DPP10) subunit preferentially form a 4:2 (Kv4.2:DPP10) channel complex. J Biol Chem 11;290(37):22724–33. doi: 10.1074/jbc.M115.646794. [PubMed: 26209633]

Laßek M, Weingarten J, Einsfelder U, Brendel P, Müller U, Volknandt W (2013) Amyloid precursor proteins are constituents of the presynaptic active zone. J Neurochem 127:48–56. doi:10.1111/jnc.12358 [PubMed: 23815291]

Laurén J, Gimbel DA, Nygaard HB, Gilbert JW, Strittmatter SM (2009) Cellular prion protein mediates impairment of synaptic plasticity by amyloid-beta oligomers. Nature 457:1128–1132. doi:10.1038/nature07761 [PubMed: 19242475]

Lee KJ, Moussa CE, Lee Y, Sung Y, Howell BW, Turner RS, Pak DT, Hoe HS (2010) Beta amyloid-independent role of amyloid precursor protein in generation and maintenance of dendritic spines. Neuroscience 169:344–356. doi:10.1016/j.neuroscience.2010.04.078 [PubMed: 20451588]

Lee L, Kosuri P, Arancio O (2014) Picomolar amyloid-β peptides enhance spontaneous astrocyte calcium transients. Journal of Alzheimer's disease. JAD 38:49–62. doi:10.3233/jad-130740 [PubMed: 23948929]

Li J, Han W, Pelkey KA, Duan J, Mao X, Wang YX, Craig MT, Dong L, Petralia RS, McBain CJ, Lu W (2017) Molecular Dissection of Neuroligin 2 and Slitrk3 Reveals an Essential Framework for GABAergic Synapse Development. Neuron 96:808–826 e808. doi:10.1016/j.neuron.2017.10.003 [PubMed: 29107521]

Liao C, Fu F, Li R, Yang WQ, Liao HY, Yan JR, Li J, Li SY, Yang X, Li DZ (2013) Loss-of-function variation in the DPP6 gene is associated with autosomal dominant microcephaly and mental retardation. Eur J Med Genet 56:484–489 [PubMed: 23832105]

Lin L, Long LK, Hatch MM, Hoffman DA (2014) DPP6 domains responsible for its localization and function. J Biol Chem 289:32153–32165 doi: 10.1074/jbc.M114.578070 [PubMed: 25190807]

Lin L, Murphy JG, Karlsson RM, Petralia RS, Gutzmann JJ, Abebe D, Wang YX, Cameron HA, Hoffman DA (2018) DPP6 Loss Impacts Hippocampal Synaptic Development and Induces Behavioral Impairments in Recognition, Learning and Memory. Front Cell Neurosci 12:84 doi: 10.3389/fncel.2018.00084 [PubMed: 29651237]

Lin L, Petralia RS, Lake R, Wang YX, Hoffman DA (2020) A novel structure associated with aging is augmented in the DPP6-KO mouse brain. Acta Neuropathol Commun 8:197. doi:10.1186/s40478-020-01065-7 [PubMed: 33225987]

Lin L, Sun W, Throesch B, Kung F, Decoster JT, Berner CJ, Cheney RE, Rudy B, Hoffman DA (2013) DPP6 regulation of dendritic morphogenesis impacts hippocampal synaptic development. Nat Commun 4:2270 doi: 10.1038/ncomms3270 [PubMed: 23912628]

Liu H, Barnes J, Pedrosa E, Herman NS, Salas F, Wang P, Zheng D, Lachman HM (2020) Transcriptome analysis of neural progenitor cells derived from Lowe syndrome induced pluripotent stem cells: identification of candidate genes for the neurodevelopmental and eye manifestations. Journal of neurodevelopmental disorders 12:14. doi:10.1186/s11689-020-09317-2 [PubMed: 32393163]

Ma D, Zhao C, Wang X, Li X, Zha Y, Zhang Y, Fu G, Liang P, Guo J, Lai D (2022) Structural basis for the gating modulation of Kv4.3 by auxiliary subunits. Cell research 32:411–414. doi:10.1038/s41422-021-00608-4 [PubMed: 34997220]

Maas C, Schiks B, Strangi RD, Hackeng TM, Bouma BN, Gebbink MF, Bouma B (2008) Identification of fibronectin type I domains as amyloid-binding modules on tissue-type plasminogen activator and three homologs. Amyloid : the international journal of experimental and clinical investigation : the official journal of the International Society of Amyloidosis 15:166–180. doi:10.1080/13506120802193498

Malloy C, Ahern M, Lin L and Hoffman DA (2022) Neuronal Roles of the Multifunctional Protein Dipeptidyl Peptidase-like 6 (DPP6). Int. J. Mol. Sci 2022, 23, 9184. Doi:10.3390/ijms23169184 [PubMed: 36012450]

Marshall CR, Noor A, Vincent JB, Lionel AC, Feuk L, Skaug J, Shago M, Moessner R, Pinto D, Ren Y, Thiruvahindrapduram B, Fiebig A, Schreiber S, Friedman J, Ketelaars CE, Vos YJ, Ficicioglu C, Kirkpatrick S, Nicolson R, Sloman L, Summers A, Gibbons CA, Teebi A, Chitayat D, Weksberg R, Thompson A, Vardy C, Crosbie V, Luscombe S, Baatjes R, Zwaigenbaum L, Roberts W, Fernandez B, Szatmari P, Scherer SW (2008) Structural variation of chromosomes in autism spectrum disorder. Am J Hum Genet 82:477–488 [PubMed: 18252227]

Maruszak A, Thuret S (2014) Why looking at the whole hippocampus is not enough-a critical role for anteroposterior axis, subfield and activation analyses to enhance predictive value of hippocampal changes for Alzheimer's disease diagnosis. Front Cell Neurosci 8:95. doi:10.3389/fncel.2014.00095 [PubMed: 24744700]

Maussion G, Cruceanu C, Rosenfeld JA, Bell SC, Jollant F, Szatkiewicz J, Collins RL, Hanscom C, Kolobova I, de Champfleur NM, Blumenthal I, Chiang C, Ota V, Hultman C, O'Dushlaine C, McCarroll S, Alda M, Jacquemont S, Ordulu Z, Marshall CR, Carter MT, Shaffer LG, Sklar P, Girirajan S, Morton CC, Gusella JF, Turecki G, Stavropoulos DJ, Sullivan PF, Scherer SW, Talkowski ME, Ernst C (2017) Implication of LRRC4C and DPP6 in neurodevelopmental disorders. Am J Med Genet A 173:395–406 [PubMed: 27759917]

Mayordomo-Cava J, Yajeya J, Navarro-López JD, Jiménez-Díaz L (2015) Amyloid-β(25–35) Modulates the Expression of GirK and KCNQ Channel Genes in the Hippocampus. PLoS One 10:e0134385. doi:10.1371/journal.pone.0134385 [PubMed: 26218288]

McNicholas K; Chen T; Abbott CA (2009) Dipeptidyl peptidase (DP) 6 and DP10: Novel brain proteins implicated in human health and disease. Clin. Chem. Lab. Med 47, 262–267. doi: 10.1515/cclm.2009.061. [PubMed: 19676137]

Mercer RC, Ma L, Watts JC, Strome R, Wohlgemuth S, Yang J, Cashman NR, Coulthart MB, Schmitt-Ulms G, Jhamandas JH, Westaway D (2013) The prion protein modulates A-type K+ currents mediated by Kv4.2 complexes through dipeptidyl aminopeptidase-like protein 6. J Biol Chem 288:37241–37255 [PubMed: 24225951]

Mijalkov M, Volpe G, Fernaud-Espinosa I, DeFelipe J, Pereira JB, Merino-Serrais P (2021) Dendritic spines are lost in clusters in Alzheimer's disease. Sci Rep 11:12350. doi:10.1038/s41598-021-91726-x [PubMed: 34117272]

Mulder SD, Nielsen HM, Blankenstein MA, Eikelenboom P, Veerhuis R (2014) Apolipoproteins E and J interfere with amyloid-beta uptake by primary human astrocytes and microglia in vitro. Glia 62:493–503. doi:10.1002/glia.22619 [PubMed: 24446231]

Musiek ES, Holtzman DM (2016) Mechanisms linking circadian clocks, sleep, and neurodegeneration. Science 354:1004–1008. doi:10.1126/science.aah4968 [PubMed: 27885006]

Musiek ES, Xiong DD, Holtzman DM (2015) Sleep, circadian rhythms, and the pathogenesis of Alzheimer disease. Exp Mol Med 47:e148. doi:10.1038/emm.2014.121 [PubMed: 25766617]

Nadal MS, Ozaita A, Amarillo Y, Vega-Saenz de Miera E, Ma Y, Mo W, Goldberg EM, Misumi Y, Ikehara Y, Neubert TA, Rudy B (2003) The CD26-related dipeptidyl aminopeptidase-like protein DPPX is a critical component of neuronal A-type K+ channels. Neuron 37:449–461 [PubMed: 12575952]

Nagele RG, D'Andrea MR, Lee H, Venkataraman V, Wang HY (2003) Astrocytes accumulate A beta 42 and give rise to astrocytic amyloid plaques in Alzheimer disease brains. Brain Res 971:197–209. doi:10.1016/s0006-8993(03)02361-8 [PubMed: 12706236]

Naujock M, Speidel A, Fischer S, Kizner V, Dorner-Ciossek C, Gillardon F (2020) Neuronal Differentiation of Induced Pluripotent Stem Cells from Schizophrenia Patients in Two-Dimensional and in Three-Dimensional Cultures Reveals Increased Expression of the Kv4.2 Subunit DPP6 That Contributes to Decreased Neuronal Activity. Stem cells and development 29:1577–1587. doi:10.1089/scd.2020.0082 [PubMed: 33143549]

Noor A, Whibley A, Marshall CR, Gianakopoulos PJ, Piton A, Carson AR, Orlic-Milacic M, Lionel AC, Sato D, Pinto D, Drmic I, Noakes C, Senman L, Zhang X, Mo R, Gauthier J, Crosbie J, Pagnamenta AT, Munson J, Estes AM, Fiebig A, Franke A, Schreiber S, Stewart AF, Roberts R, McPherson R, Guter SJ, Cook EH Jr., Dawson G, Schellenberg GD, Battaglia A, Maestrini E, Jeng L, Hutchison T, Rajcan-Separovic E, Chudley AE, Lewis SM, Liu X, Holden JJ, Fernandez B, Zwaigenbaum L, Bryson SE, Roberts W, Szatmari P, Gallagher L, Stratton MR, Gecz J, Brady AF, Schwartz CE, Schachar RJ, Monaco AP, Rouleau GA, Hui CC, Lucy Raymond F, Scherer SW,

Vincent JB (2010) Disruption at the PTCHD1 Locus on Xp22.11 in Autism spectrum disorder and intellectual disability. Sci Transl Med 2:49ra68

Oblak AL, Lin PB, Kotredes KP, Pandey RS, Garceau D, Williams HM, Uyar A, O'Rourke R, O'Rourke S, Ingraham C, Bednarczyk D, Belanger M, Cope ZA, Little GJ, Williams SG, Ash C, Bleckert A, Ragan T, Logsdon BA, Mangravite LM, Sukoff Rizzo SJ, Territo PR, Carter GW, Howell GR, Sasner M, Lamb BT (2021) Comprehensive Evaluation of the 5XFAD Mouse Model for Preclinical Testing Applications: A MODEL-AD Study. Front Aging Neurosci 13:713726. doi:10.3389/fnagi.2021.713726 [PubMed: 34366832]

Osborn LM, Kamphuis W, Wadman WJ, Hol EM (2016) Astrogliosis: An integral player in the pathogenesis of Alzheimer's disease. Prog Neurobiol 144:121–141. doi:10.1016/j.pneurobio.2016.01.001 [PubMed: 26797041]

Paranjape GS, Gouwens LK, Osborn DC, Nichols MR (2012) Isolated amyloid-β(1–42) protofibrils, but not isolated fibrils, are robust stimulators of microglia. ACS chemical neuroscience 3:302–311. doi:10.1021/cn2001238 [PubMed: 22860196]

Parihar MS, Brewer GJ (2010) Amyloid-β as a modulator of synaptic plasticity. Journal of Alzheimer's disease : JAD 22:741–763. doi:10.3233/jad-2010-101020 [PubMed: 20847424]

Petralia RS, Mattson MP, Yao PJ (2014) Communication breakdown: the impact of ageing on synapse structure. Ageing research reviews 14:31–42. doi:10.1016/j.arr.2014.01.003 [PubMed: 24495392]

Petralia RS, Wang YX, Hua F, Yi Z, Zhou A, Ge L, Stephenson FA, Wenthold RJ (2010) Organization of NMDA receptors at extrasynaptic locations. Neuroscience 167:68–87. doi:10.1016/j.neuroscience.2010.01.022 [PubMed: 20096331]

Petralia RS, Wang YX, Mattson MP, Yao PJ (2015) Structure, Distribution, and Function of Neuronal/Synaptic Spinules and Related Invaginating Projections. Neuromolecular medicine 17:211–240. doi:10.1007/s12017-015-8358-6 [PubMed: 26007200]

Petralia RS, Wang YX, Mattson MP, Yao PJ (2018) Invaginating Structures in Mammalian Synapses. Frontiers in synaptic neuroscience 10:4. doi:10.3389/fnsyn.2018.00004 [PubMed: 29674962]

Petralia RS, Yao PJ, Kapogiannis D, Wang YX (2021) Invaginating Structures in Synapses - Perspective. Frontiers in synaptic neuroscience 13:685052. doi:10.3389/fnsyn.2021.685052 [PubMed: 34108873]

Petralia RS, Wang YX (2021) Review of postembedding immunogold methods for the study of neuronal structures. Frontiers in neuroanatomy 15:763427 [PubMed: 34720893]

Pons V, Lévesque P, Plante MM, Rivest S (2021) Conditional genetic deletion of CSF1 receptor in microglia ameliorates the physiopathology of Alzheimer's disease. Alzheimers Res Ther. 5;13(1):8. doi: 10.1186/s13195-020-00747-7. [PubMed: 33402196]

Pottier C, Ren Y, Perkerson RB 3rd, Baker M, Jenkins GD, van Blitterswijk M, DeJesus-Hernandez M, van Rooij JGJ, Murray ME, Christopher E, McDonnell SK, Fogarty Z, Batzler A, Tian S, Vicente CT, Matchett B, Karydas AM, Hsiung GR, Seelaar H, Mol MO, Finger EC, Graff C, Oijerstedt L, Neumann M, Heutink P, Synofzik M, Wilke C, Prudlo J, Rizzu P, Simon-Sanchez J, Edbauer D, Roeber S, Diehl-Schmid J, Evers BM, King A, Mesulam MM, Weintraub S, Geula C, Bieniek KF, Petrucelli L, Ahern GL, Reiman EM, Woodruff BK, Caselli RJ, Huey ED, Farlow MR, Grafman J, Mead S, Grinberg LT, Spina S, Grossman M, Irwin DJ, Lee EB, Suh E, Snowden J, Mann D, Ertekin-Taner N, Uitti RJ, Wszolek ZK, Josephs KA, Parisi JE, Knopman DS, Petersen RC, Hodges JR, Piguet O, Geier EG, Yokoyama JS, Rissman RA, Rogaeva E, Keith J, Zinman L, Tartaglia MC, Cairns NJ, Cruchaga C, Ghetti B, Kofler J, Lopez OL, Beach TG, Arzberger T, Herms J, Honig LS, Vonsattel JP, Halliday GM, Kwok JB, White CL 3rd, Gearing M, Glass J, Rollinson S, Pickering-Brown S, Rohrer JD, Trojanowski JQ, Van Deerlin V, Bigio EH, Troakes C, Al-Sarraj S, Asmann Y, Miller BL, Graff-Radford NR, Boeve BF, Seeley WW, Mackenzie IRA, van Swieten JC, Dickson DW, Biernacka JM, Rademakers R (2019) Genome-wide analyses as part of the international FTLD-TDP whole-genome sequencing consortium reveals novel disease risk factors and increases support for immune dysfunction in FTLD. Acta Neuropathol 137:879–899. doi:10.1007/s00401-019-01962-9 [PubMed: 30739198]

Prontera P, Napolioni V, Ottaviani V, Rogaia D, Fusco C, Augello B, Serino D, Parisi V, Bernardini L, Merla G, Cavanna AE, Donti E (2014) DPP6 gene disruption in a family with Gilles de la Tourette syndrome. Neurogenetics 15:237–242 [PubMed: 25129042]

Puzzo D, Privitera L, Palmeri A (2012) Hormetic effect of amyloid-β peptide in synaptic plasticity and memory. Neurobiol Aging 33:1484 e1415–1424. doi:10.1016/j.neurobiolaging.2011.12.020

Rademakers R, Cruts M, Sleegers K, Dermaut B, Theuns J, Aulchenko Y, Weckx S, De Pooter T, Van den Broeck M, Corsmit E, De Rijk P, Del-Favero J, van Swieten J, van Duijn CM, Van Broeckhoven C (2005) Linkage and association studies identify a novel locus for Alzheimer disease at 7q36 in a Dutch population-based sample. Am J Hum Genet 77:643–652. doi:10.1086/491749 [PubMed: 16175510]

Rahman MM, Uddin KF, Al Jezawi NK, Karuvantevida N, Akter H, Dity NJ, Rahaman MA, Begum M, Rahaman MA, Baqui MA, Salwa Z, Islam S, Woodbury-Smith M, Basiruzzaman M, Uddin M (2019) Gonadal mosaicism of large terminal de novo duplication and deletion in siblings with variable intellectual disability phenotypes. Mol Genet Genomic Med 7:e00954 [PubMed: 31475484]

Refinetti R (2004) Daily activity patterns of a nocturnal and a diurnal rodent in a seminatural environment. Physiol Behav 82:285–294. doi:10.1016/j.physbeh.2004.03.015 [PubMed: 15276790]

Ren X; Hayashi Y; Yoshimura N; Takimoto K (2005) Transmembrane interaction mediates complex formation between peptidase homologues and Kv4 channels. Mol. Cell Neurosci 29, 320–332. doi: 10.1016/j.mcn.2005.02.003 [PubMed: 15911355]

Ricciarelli R, Puzzo D, Bruno O, Canepa E, Gardella E, Rivera D, Privitera L, Domenicotti C, Marengo B, Marinari UM, Palmeri A, Pronzato MA, Arancio O, Fedele E (2014) A novel mechanism for cyclic adenosine monophosphate-mediated memory formation: Role of amyloid beta. Ann Neurol 75:602–607. doi:10.1002/ana.24130 [PubMed: 24591104]

Ries M, Sastre M (2016) Mechanisms of Aβ Clearance and Degradation by Glial Cells. Front Aging Neurosci 8:160. doi:10.3389/fnagi.2016.00160 [PubMed: 27458370]

Schuff N, Woerner N, Boreta L, Kornfield T, Shaw LM, Trojanowski JQ, Thompson PM, Jack CR Jr., Weiner MW (2009) MRI of hippocampal volume loss in early Alzheimer's disease in relation to ApoE genotype and biomarkers. Brain: a journal of neurology 132:1067–1077. doi:10.1093/brain/awp007 [PubMed: 19251758]

Schultz C, Del Tredici K, Braak H (2004) Neuropathology of Alzheimer's Disease. Book: Alzheimer's Disease A physician's guide to practical management P21–31

Serôdio P, Rudy B (1998) Differential expression of Kv4 K+ channel subunits mediating subthreshold transient K+ (A-type) currents in rat brain. J Neurophysiol 79:1081–1091. doi:10.1152/jn.1998.79.2.1081 [PubMed: 9463463]

Shoji H, Takao K, Hattori S, Miyakawa T (2016) Age-related changes in behavior in C57BL/6J mice from young adulthood to middle age. Mol Brain 9:11. doi:10.1186/s13041-016-0191-9 [PubMed: 26822304]

Sos KE, Mayer MI, Takács VT, Major A, Bardóczi Z, Beres BM, Szeles T, Saito T, Saido TC, Mody I, Freund TF, Nyiri G (2020) Amyloid β induces interneuron-specific changes in the hippocampus of APPNL-F mice. PLoS One 15:e0233700. doi:10.1371/journal.pone.0233700 [PubMed: 32469963]

Soto C, Pritzkow S (2018) Protein misfolding, aggregation, and conformational strains in neurodegenerative diseases. Nat Neurosci 21:1332–1340. doi:10.1038/s41593-018-0235-9 [PubMed: 30250260]

Spanic E, Langer Horvat L, Hof PR, Simic G (2019) Role of Microglial Cells in Alzheimer's Disease Tau Propagation. Front Aging Neurosci 11:271. doi:10.3389/fnagi.2019.00271 [PubMed: 31636558]

Strop P, Bankovich AJ, Hansen KC, Garcia KC, Brunger AT (2004) Structure of a human A-type potassium channel interacting protein DPPX, a member of the dipeptidyl aminopeptidase family. Journal of molecular biology 343:1055–1065. doi:10.1016/j.jmb.2004.09.003 [PubMed: 15476821]

Sun W, Maffie JK, Lin L, Petralia RS, Rudy B, Hoffman DA (2011) DPP6 establishes the A-type K(+) current gradient critical for the regulation of dendritic excitability in CA1 hippocampal neurons. Neuron 71:1102–1115 [PubMed: 21943606]

Takahashi RH, Capetillo-Zarate E, Lin MT, Milner TA, Gouras GK (2013) Accumulation of intraneuronal beta-amyloid 42 peptides is associated with early changes in microtubule-associated

protein 2 in neurites and synapses. PLoS One 8:e51965. doi:10.1371/journal.pone.0051965 [PubMed: 23372648]

Teng XC, Dayhoff-Brannigan M, Cheng WC, Gilbert CE, Sing CN, Diny NL, Wheelan SJ, Dunham MJ, Boeke JD, Pineda FJ, Hardwick JM (2013) Genome-wide consequences of deleting any single gene. Mol Cell 21;52(4):485–94. doi: 10.1016/j.molcel.2013.09.026 [PubMed: 24211263]

Terry RD, Gonatas NK, Weiss M (1964) Ultrastructural studies in Alzheimer's presenile dementia. Am J Pathol 44(2): 269–297. [PubMed: 14119171]

Torroja L, Packard M, Gorczyca M, White K, Budnik V (1999) The Drosophila beta-amyloid precursor protein homolog promotes synapse differentiation at the neuromuscular junction. J Neurosci 19:7793–7803. doi:10.1523/jneurosci.19-18-07793.1999 [PubMed: 10479682]

Uddin MS, Tewari D, Mamun AA, Kabir MT, Niaz K, Wahed MII, Barreto GE, Ashraf GM (2020) Circadian and sleep dysfunction in Alzheimer's disease. Ageing research reviews 60:101046. doi:10.1016/j.arr.2020.101046 [PubMed: 32171783]

Um JW, Strittmatter SM (2013) Amyloid-β induced signaling by cellular prion protein and Fyn kinase in Alzheimer disease. Prion 7:37–41. doi:10.4161/pri.22212 [PubMed: 22987042]

Verite J, Janet T, Julian A, Chassaing D, Page G, Paccalin M (2017) Peripheral Blood Mononuclear Cells of Alzheimer's Disease Patients Control CCL4 and CXCL10 Levels in a Human Blood Brain Barrier Model. Current Alzheimer research 14:1215–1228. doi:10.2174/1567205014666170417110337 [PubMed: 28413983]

Vermunt L, Veal CD, Ter Meulen L, Chrysostomou C, van der Flier W, Frisoni GB, Guessous I, Kivipelto M, Marizzoni M, Martinez-Lage P, Molinuevo JL, Porteous D, Ritchie K, Scheltens P, Ousset PJ, Ritchie CW, Luscan G, Brookes AJ, Visser PJ (2018) European Prevention of Alzheimer's Dementia Registry: Recruitment and prescreening approach for a longitudinal cohort and prevention trials. Alzheimers Dement 14:837–842. doi:10.1016/j.jalz.2018.02.010 [PubMed: 29604264]

Videnovic A, Lazar AS, Barker RA, Overeem S (2014) 'The clocks that time us'--circadian rhythms in neurodegenerative disorders. Nature reviews Neurology 10:683–693. doi:10.1038/nrneurol.2014.206 [PubMed: 25385339]

Vijayakumar A, Vijayakumar A (2013) Comparison of hippocampal volume in dementia subtypes. ISRN radiology 2013:174524. doi:10.5402/2013/174524 [PubMed: 24959551]

Villa C, Suphesiz H, Combi R, Akyuz E (2020) Potassium channels in the neuronal homeostasis and neurodegenerative pathways underlying Alzheimer's disease: An update. Mechanisms of ageing and development 185:111197. doi:10.1016/j.mad.2019.111197 [PubMed: 31862274]

Wagner KD, Wagner N (2022) The Senescence Markers p16INK4A, p14ARF/p19ARF, and p21 in Organ Development and Homeostasis. Cells 19;11(12):1966. doi: 10.3390/cells11121966. [PubMed: 35741095]

Wang WC, Cheng CF, Tsaur ML (2015) Immunohistochemical localization of DPP10 in rat brain supports the existence of a Kv4/KChIP/DPPL ternary complex in neurons. J Comp Neurol 1;523(4):608–28. doi: 10.1002/cne.23698. [PubMed: 25355692]

Wang Z, Yang L, Zheng H (2012) Role of APP and Aβ in synaptic physiology. Current Alzheimer research 9:217–226. doi:10.2174/156720512799361691 [PubMed: 21605029]

Weingarten J, Weingarten M, Wegner M, Volknandt W (2017) APP-A Novel Player within the Presynaptic Active Zone Proteome. Front Mol Neurosci 10:43. doi:10.3389/fnmol.2017.00043 [PubMed: 28265241]

Weldemichael DA, Grossberg GT (2010) Circadian rhythm disturbances in patients with Alzheimer's disease: a review. International journal of Alzheimer's disease 2010. doi:10.4061/2010/716453

Wu HY, Kuo PC, Wang YT, Lin HT, Roe AD, Wang BY, Han CL, Hyman BT, Chen YJ, Tai HC (2018) β-Amyloid Induces Pathology-Related Patterns of Tau Hyperphosphorylation at Synaptic Terminals. J Neuropathol Exp Neurol 77:814–826. doi:10.1093/jnen/nly059 [PubMed: 30016458]

Zelaya MV, Pérez-Valderrama E, de Morentin XM, Tuñon T, Ferrer I, Luquin MR, Fernandez-Irigoyen J, Santamaría E (2015) Olfactory bulb proteome dynamics during the progression of sporadic Alzheimer's disease: identification of common and distinct olfactory targets across Alzheimer-

related co-pathologies. Oncotarget 6:39437–39456. doi:10.18632/oncotarget.6254 [PubMed: 26517091]

Zhang J, Qiu W, Hu F, Zhang X, Deng Y, Nie H, Xu R (2021) The rs2619566, rs10260404, and rs79609816 Polymorphisms Are Associated With Sporadic Amyotrophic Lateral Sclerosis in Individuals of Han Ancestry From Mainland China. Frontiers in genetics 12:679204. doi:10.3389/fgene.2021.679204 [PubMed: 34421992]

Zheng C, Zhou XW and Wang JZ (2016) The dual roles of cytokines in Alzheimer's disease: update on interleukins, TNF-α, TGF-β and IFN-γ. Translational Neurodegeneration 5:7 DOI 10.1186/s40035-016-0054-4 [PubMed: 27054030]

Zhou L, Miller BL, McDaniel CH, Kelly L, Kim OJ, Miller CA (1998) Frontotemporal dementia: neuropil spheroids and presynaptic terminal degeneration. Ann Neurol 44:99109. doi:10.1002/ana.410440116

Zhu M, Allard JS, Zhang Y, Perez E, Spangler EL, Becker KG, Rapp PR (2014) Age-related brain expression and regulation of the chemokine CCL4/MIP-1β in APP/PS1 double-transgenic mice. J Neuropathol Exp Neurol 73:362–374. doi:10.1097/nen.0000000000000060 [PubMed: 24607962]

**Highlights:**

- Aging DPP6-KO mice show reduced hippocampal volume as found in AD
- Hyperphosphorylated tau and amyloid accumulate in aging DPP6-KO mice
- APP accumulation in presynaptic terminals is associated with increased invaginations
- Neuroinflammation with increased cytokines and astroglia/microglia in DPP6-KO
- Similar novel NeuN-labeled structures are found in hippocampal CA1 of AD donors

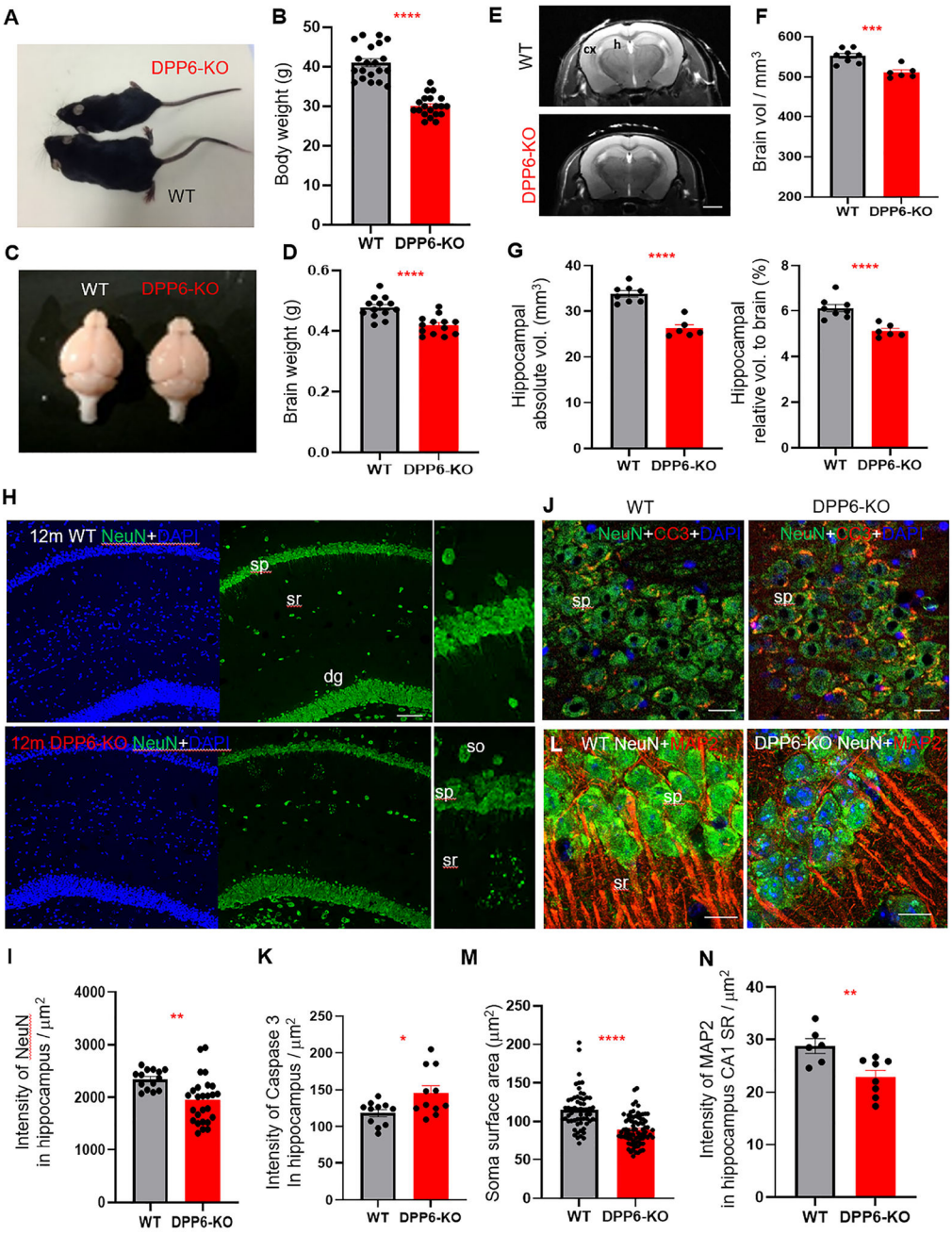


**Figure 1. DPP6-KO mice have smaller brains in *in vivo* MRI studies and show strucrtural changes in the hippocampus**

**A-B:** Body weight of 12-month-old DPP6-KO mice is significantly reduced compared to WT (n=20 mice each, $p$ <0.0001). **C-D:** 12-month-old DPP6-KO mice also show decreased brain weight compared to WT (n=13 mice each, $p$ <0.0001). **E-F**: *In vivo* MRI reveals a significant decrease in total brain volume in DPP6-KO mice (WT n=8; DPP6-KO n=6, $p$ <0.001), scale bar:2 mm. **G:** Hippocampal absolute volume and relative volume are decreased in DPP6-KO live mice compared to WT (Absolute volume, $p$ <0.0001; right: Relative volume, $p$ <0.0001). **H-I**: Immunofluorescence labeling (IF) shows that there is

less NeuN (green, 1:500) in hippocampus of 12-month-old DPP6-KO mice compared to WT (WT n=14; DPP6-KO n=26 sections, $p$ <0.01). CA1 region is shown in H. Scale bars:50 μm. **J-K:** More apoptotic neurons in 12-month-old DPP6-KO in the hippocampal area (apoptosis marker cleaved caspase3, CC3, red) compared to WT. J shows the CA3 stratum pyramidale and K shows the intensity of labeling for CC3 in the entire hippocampal stratum pyramidale (WT n=11, DPP6-KO n=11 sections, $p$<0.05). Scale bars:20 μm. **L-N:** DPP6-KO CA1 pyramidal cell somas appear shrunken, based on NeuN labeling (green) with fewer apical dendrites with MAP2 labeling (red) in 12-month-old DPP6-KO compared to the WT. Also, the soma surface area of CA1 stratum pyramidale in DPP6-KO is significantly smaller than in WT (Figure 1M, WT n=60, DPP6-KO n=80 cells, $p$ <0.0001), and the MAP2 intensity in the CA1 stratum radiatum is less in DPP6-KO mice (Figure 1N, WT n=6, DPP6-KO n=8 sections, $p$ <0.01), 3–5 mice were examined in each IF experiment. cx, cortex; dg, dentate gyrus; h, hippocampus; so, stratum oriens; sp, stratum pyramidale; sr, stratum radiatum. Scale bars:5 μm. Nuclei were counterstained with DAPI in blue. Error bars represent ±SEM. Statistical significance was evaluated by Student's t test. *$p$ < 0.05, **$p$ < 0.01, ***$p$ < 0.001, ****$p$ < 0.0001.

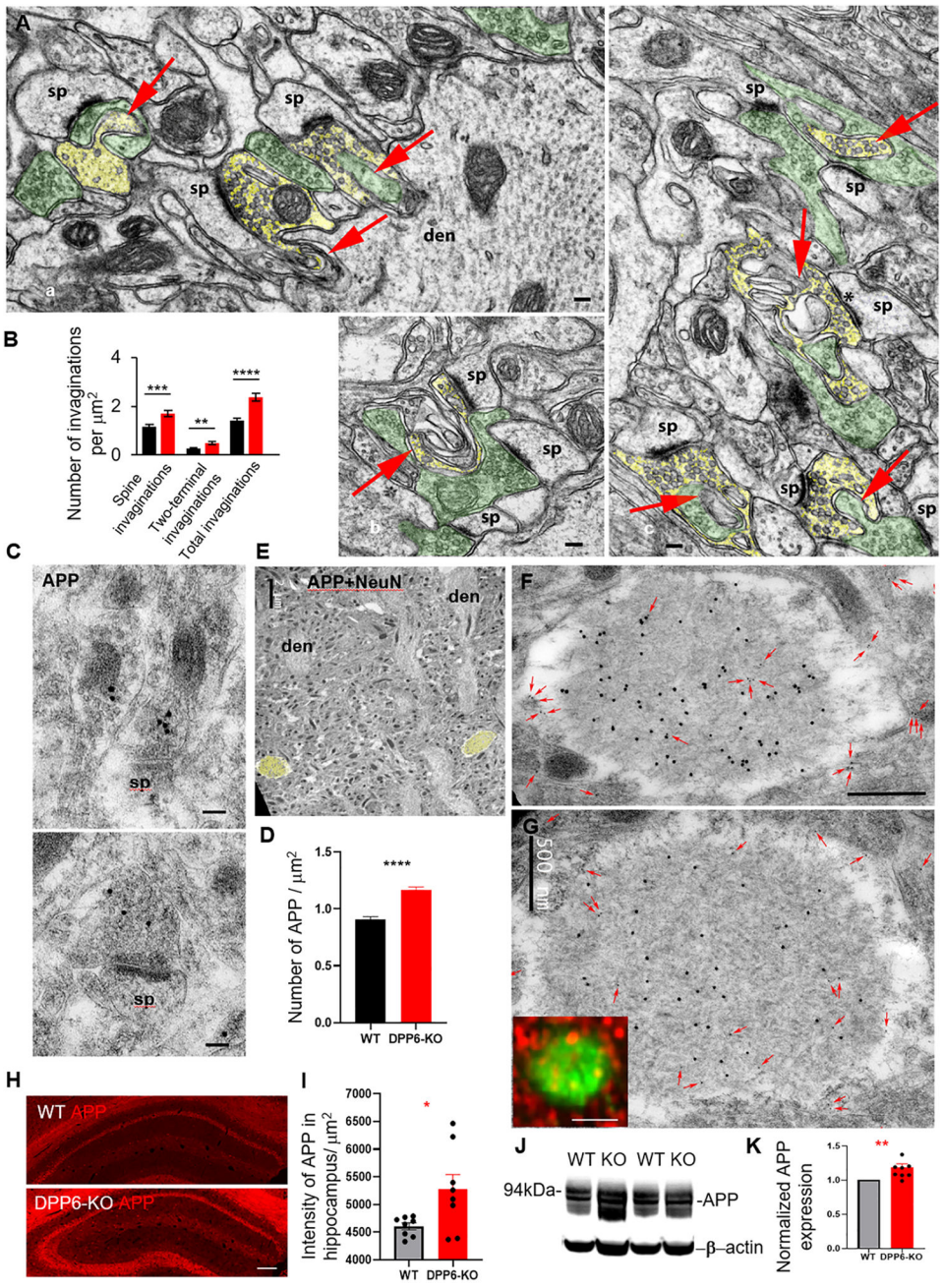


**Figure 2. APP accumulation in the presynaptic terminals is associated with increased invaginations and novel structures in 12-month DPP6-KO hippocampus**

**A**: Electron microscopy reveals that invaginating structures (arrows) are found commonly in the presynaptic terminals in the CA1 region of the hippocampus. Some reciprocal invaginating terminals (see text for details) are colored yellow and green for clarity. den, large apical dendrite of the CA1 stratum radiatum; sp, spines; asterisk, perforated postsynaptic density. Scale bars:100 nm. **B**: Graph shows an increase in the number of invaginations in the 12-month DPP6-KO compared to the WT for spine invaginations, two-terminal invaginations, and total invaginations (n=156 images for WT, n=127 images

for DPP6-KO, from 2 mice each. $p$ <0.001). **C**: Immunogold localization (20 nm gold) for APP in the CA1 region of the hippocampus. All gold particles in these images are in presynaptic terminals. sp, spines. Scale bar:100 nm. **D**: Graph shows that the number of APP gold particles in 12-month DPP6-KO is significantly increased compared to WT. Most gold particles are in presynaptic terminals (n=188 images for WT, n=201 images for DPP6-KO mice, from 2 mice each, $p$ <0.001). **E,F,G:** Immunogold labeling for APP (10 nm; all immunogold particles in image are labeled with small arrows) in the hippocampus CA1 from DPP6-KO mice is common in the novel swellings labeled with NeuN (20 nm immunogold; colored yellow in the low magnification image, **E**). F is a high-magnification image of the left swelling shown in E. The swelling in G is from a second DPP6-KO mouse. Scale bars are 2 μm for E and 500 nm for F and G; these scale bars were retained from the original raw image files. An inset in G shows an immunofluorescence image of a single NeuN+-large punctum corresponding to a swelling, labeled with APP in red and NeuN in green, scale bar:2 μm. **H,I.** In the hippocampus of 12-month-old DPP6-KO brain sections, IF for APP (red) is significantly enhanced compared to WT (n=8 sections, $p$ <0.01). scale bar:100 μm. **J,K**: Immunoblot shows that total expression of APP in 12-month-old DPP6-KO hippocampus is increased compared to WT (n=8 sections, $p$ <0.01). 4 mice were examined in the IF experiment. Error bars represent ±SEM. Statistical significance was evaluated by Student's t test. *$p$ < 0.05, **$p$ < 0.01, ***$p$ < 0.001, ****$p$ < 0.0001.

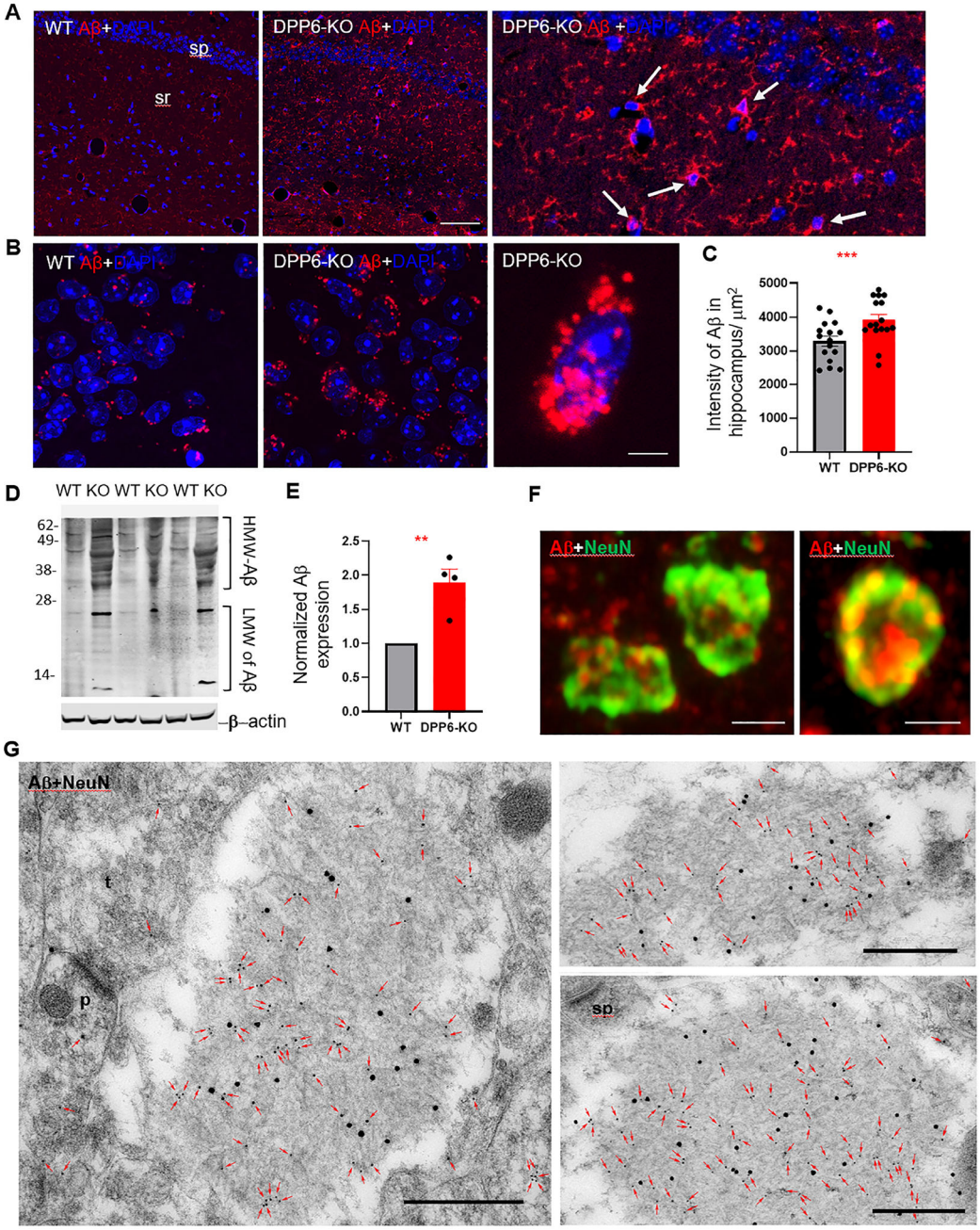


**Figure 3. DPP6 deficiency induces amyloid deposition in hippocampus and novel NeuN+ structures**

**A:** IF for Aβ (red) shows more accumulation in the hippocampus CA1 of 12-month-old DPP6-KO mice compared to WT. sp, stratum pyramidale; sr, stratum radiatum. Scale bars:50 μm. **B:** Low and high magnification images show the accumulation of Aβ in the cytoplasm of CA1 stratum pyramidale neurons of 12-month-old DPP6-KO. Scale bar:5 μm. **C:** Graph shows that the intensity of Aβ is significantly enhanced in 12-month DPP6-KO mice compared to WT (n=16 each, $p$ <0.01). **D-E**: Western blot shows that low and high molecular weight forms (LMW and HMW) of Aβ are more highly expressed in 12-month-

old DPP6-KO hippocampal lysate compared to WT (n=4 mice each, $p$ <0.05). **F:** IF shows Aβ (red) partially colocalized with the novel NeuN+ (green) structures. Note the greater colocalization seen in the right image. Scale bars:2 μm. 3–5 mice were examined in each IF experiment. **G**: Immunogold labeling for Aβ (10 nm; all immunogold particles in image are labeled with small arrows) in the hippocampus CA1 can be common in the novel swellings labeled with NeuN (20 nm immunogold) in both WT (left and top, right image) and KO (bottom, right image). p, postsynaptic dendrite; sp, spine; t, presynaptic terminal. Scale bar is 500 nm in the left image and in the top, right image for both right images. Error bars represent ±SEM. Statistical significance was evaluated by Student's t test. *$p$ < 0.05, **$p$ < 0.01, ***$p$ < 0.001, ****$p$ < 0.0001.

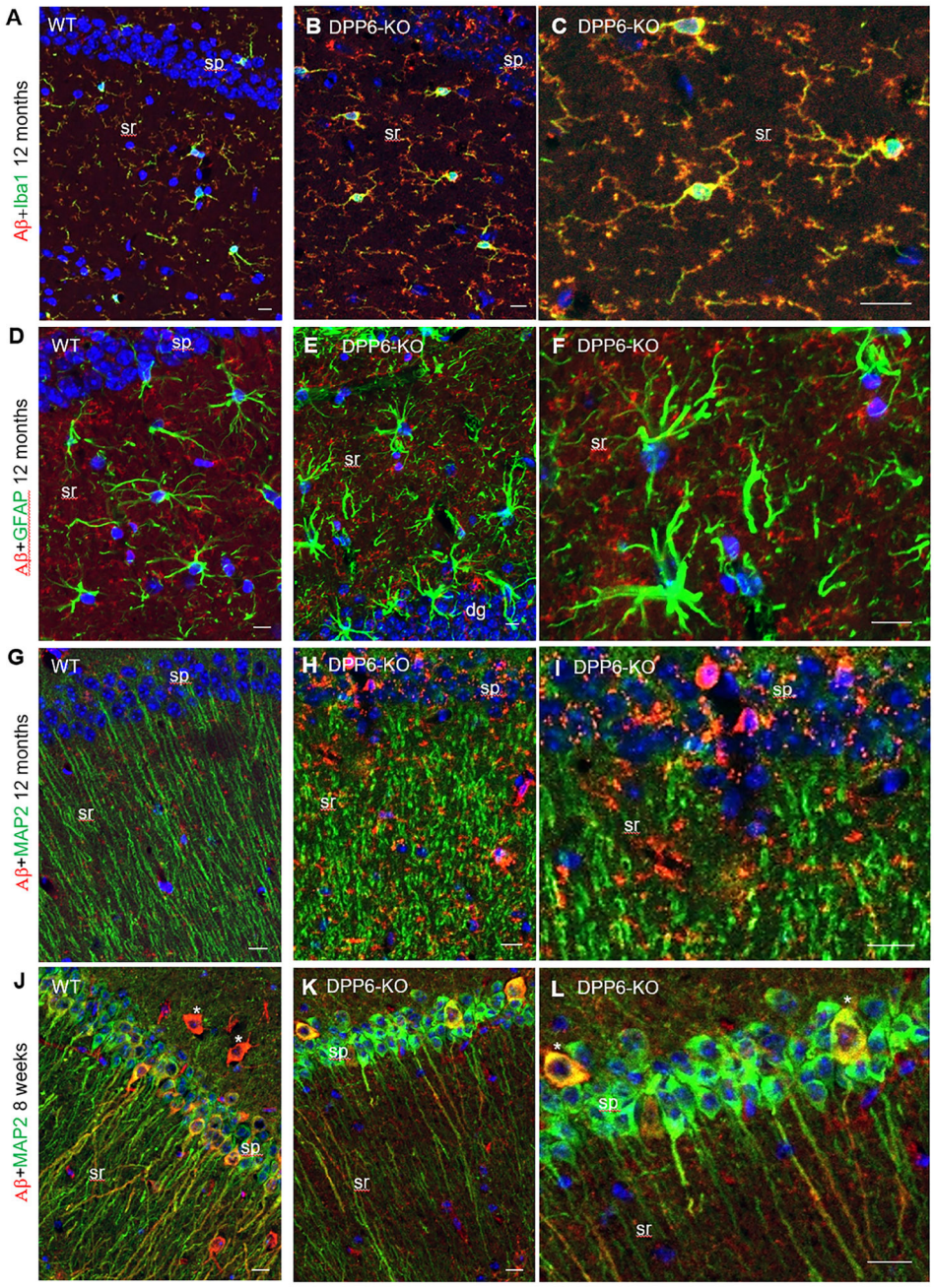


**Figure 4. Aβ is associated with microglia and astrocytes**

**A,B**: IF in 12-month-old WT (**A**) and DPP6-KO (**B**) mouse brain sections labeled for Aβ (red) and microglia marker Iba1 (green). **C**: A high magnification image of the DPP6-KO shows the close colocalization of Aβ-labeling with Iba1-labeling in microglia somas and processes. **D,E:** IF in 12-month-old WT (**D**) and DPP6-KO (**E**) mouse brain sections labeled for Aβ (red) and the astrocyte marker GFAP (green). **F**: A high magnification image of the DPP6-KO shows Aβ-labeled small processes associated with astrocyte processes. **G,H**: IF in 12-month-old WT (**G**) and DPP6-KO (**H**) mouse brain sections labeled with Aβ (red) with MAP2 (green). **I**: A high magnification image of the DPP6-KO shows that most labeling for

Aβ is outside of the MAP2-labeled dendrite profiles; few Aβ-labeled puncta are colocalized with these dendrites, which appear irregularly shaped in the KO (dysmorphic). **J-L (J**, WT; **K,L**, DPP6-KO): In contrast, in the 8-week-old WT and DPP6-KO mouse brain, IF using the same antibodies to Aβ and MAP2 as used in the 12-month-old WT and DPP6-KO show some diffuse labeling for Aβ in some pyramidal neuron somas and apical dendrites, which appear more normal in structure than those in the 12-month-old DPP6-KO mice. Also, labeling for Aβ is concentrated in distinct interneurons (asterisks). 3 mice have been examined for each IF experiment. sp, stratum pyramidale; sr, stratum radiatum. Scale bar:20 μm.

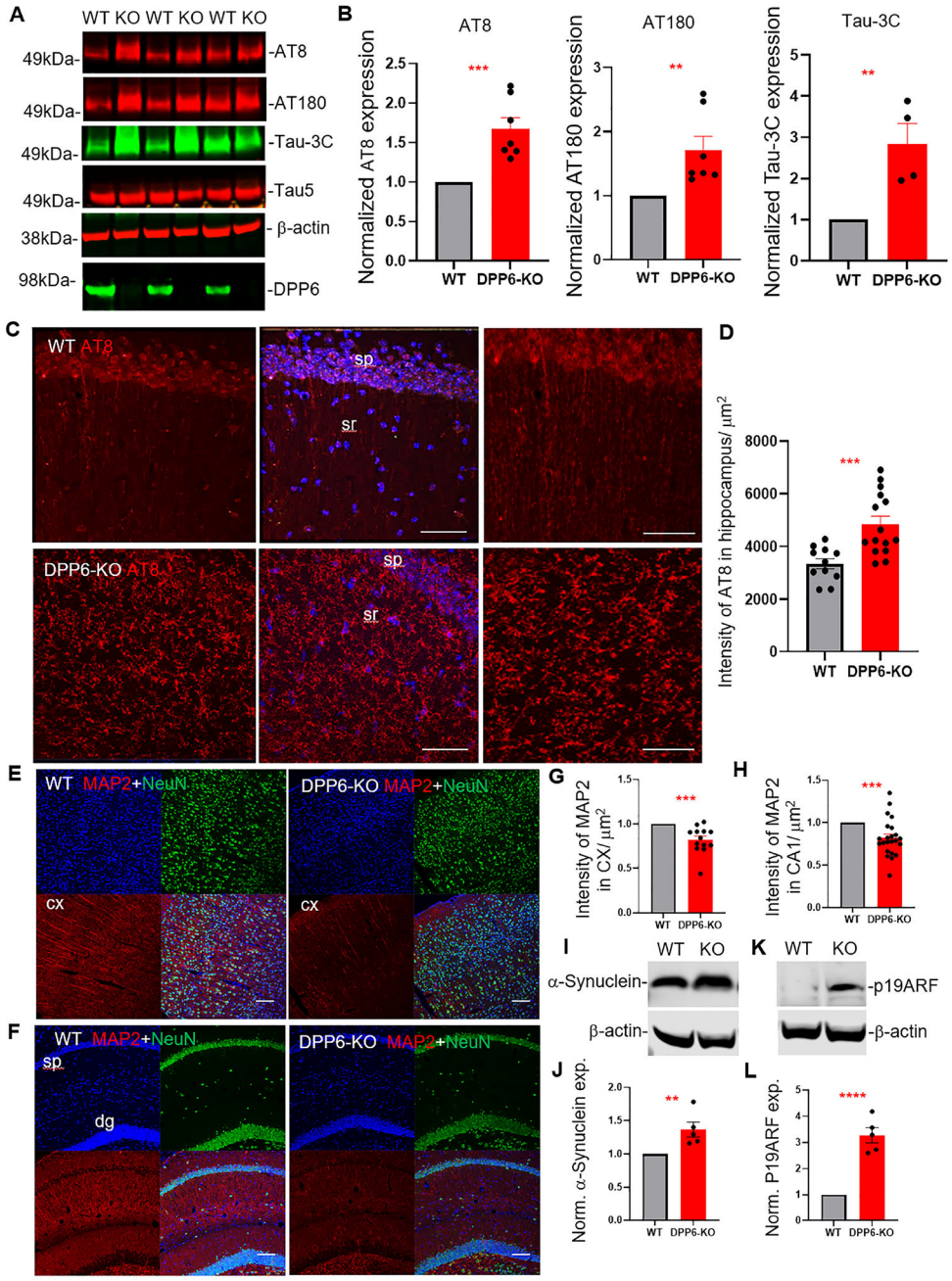


**Figure 5. Hyper-phosphorylated tau is increased in 12-month DPP6-KO mouse hippocampus, ultimately leading to degeneration**

**A-B**: Western blots show that in 12-month-old DPP6-KO hippocampal lysate, the total expression levels of AT8, AT180 and Tau3C are significantly increased compared to WT. There are no significant changes for the total protein levels of Tau5 and actin (control) (AT8 n=7 mice, $p$ <0.001; AT180 n=7 mice, $p$ <0.01 and Tau3C n=4 mice, $p$< 0.01).

**C-D:** IF labeling with AT8 (red) in the hippocampal CA1 shows that the intensity of AT8 is increased in 12-month-old DPP6-KO mice compared with WT (WT n=11, DPP6-KO n=15 sections, $p$ <0.001) and there is a change in expression pattern (see Results). Scale

bar:20μm. **E-F:** IF label with MAP2 (red) and NeuN (green) in cortex (**E**) and hippocampus (**F**) shows an opposite pattern from the AT8, with abundant labeling of MAP2 in the apical dendrites and associated neuropil in the 12-month-old WT mice, and much less MAP2 labeling in 12-month-old DPP6-KO mice. Scale bar:50μm. **G,H**: Intensity of MAP2 labeling in the cerebral cortex (WT n=13, DPP6-KO n=13 sections, $p<0.001$) and CA1 (WT n=23, DPP6-KO n=23 sections, $p<0.001$) is significantly decreased in the DPP6-KO compared to WT. **I-L**: Western blots show that in 12-month-old DPP6-KO hippocampal lysate, the total protein level of α-synuclein (**I,J**, n=5 mice, $p<0.01$) and P19ARF (**K,L**, 1:1000, n=5 mice, $p<0.001$) is significantly increased in DPP6-KO mice compared to WT. Nuclei were counterstained with DAPI in blue. 3–5 mice were examined in each IF experiment. cx, cortex; dg, dentate gyrus; sp, stratum pyramidale; sr, stratum radiatum. Error bars represent ±SEM. Statistical significance was evaluated by Student's t test. *$p < 0.05$, **$p < 0.01$, ***$p < 0.001$, ****$p < 0.0001$.

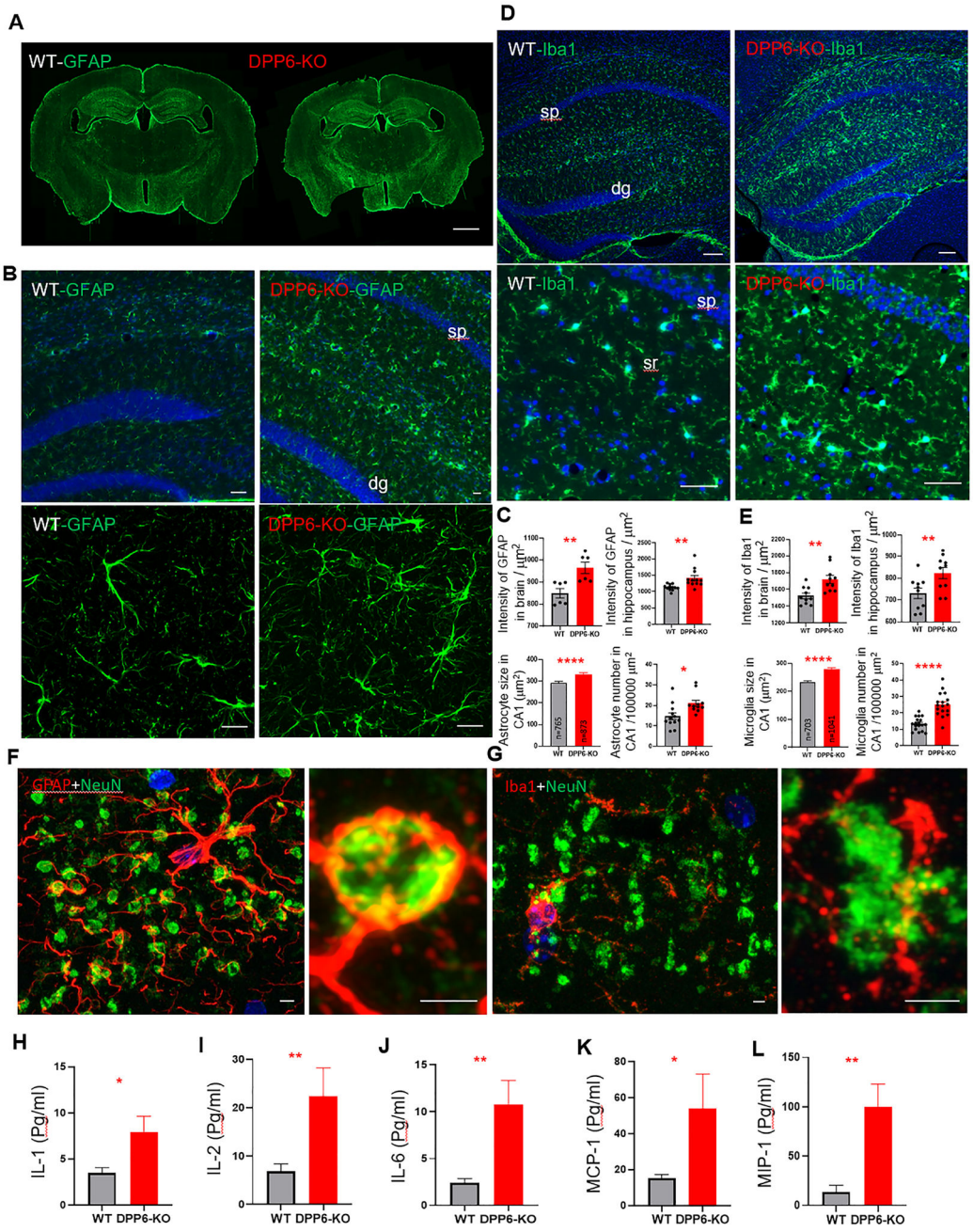


**Figure 6. Activated astrocytes and microglia cells are dramatically increased in 12-month DPP6-KO brain and associated with the novel NeuN+ structures**

**A:** Whole brain sections labeled with the astrocyte marker GFAP (green) in 12-month-old WT and DPP6-KO mice. Scale bar:1mm. **A-C**: In 12-month-old DPP6-KO mice, whole brain (**A**) and hippocampal sections (**B**) show higher intensity for GFAP (Figure 6C, $p < 0.01$) and astrocytes are increased in size and number in DPP6-KO CA1 compared to WT (Figure 6C, $p < 0.0001$ and $p < 0.05$); magnified in lower panels of Figure 6B). Scale bar:20µm. **D-E**: IF with microglia marker Iba1 (green) labeled in hippocampus of 12-month-old DPP6-KO mice; the high-magnification lower panels show the irregular and

sometimes enlarged, activated microglia, compared to the WT mice hippocampus, which shows more typical, normal microglia. The intensity of Iba1 in both brain and hippocampus are significantly higher in DPP6-KO than in the WT (Figure 6E, $p$ <0.01), and microglia are increased in size and number in DPP6-KO CA1 compared to WT (Figure 6E, $p$<0.0001). Scale bar:100μm for low and 20 μm for high magnification. **F**: IF shows that the GFAP+ astrocytes can directly surround the novel NeuN+ large puncta, sometimes as distinct ring-shaped processes. **G**: IF shows the Iba1+ microglia associated with the novel NeuN+ large puncta. Scale bar=2μm, (F-G). 3–5 mice were examined in each IF experiment**. H-L:** Pro- and anti-inflammatory cytokine levels are significantly higher in 12-month-old DPP6-KO mouse blood serum (n=10 mice each of WT and DPP6-KO, $p$ <0.01) compared to WT. Nuclei were counterstained with DAPI in blue. dg, dentate gyrus; sp, stratum pyramidale; sr, stratum radiatum. Error bars represent ±SEM. Statistical significance was evaluated by Student's t test. *$p$ < 0.05, **$p$ < 0.01, ***$p$ < 0.001, ****$p$ < 0.0001.

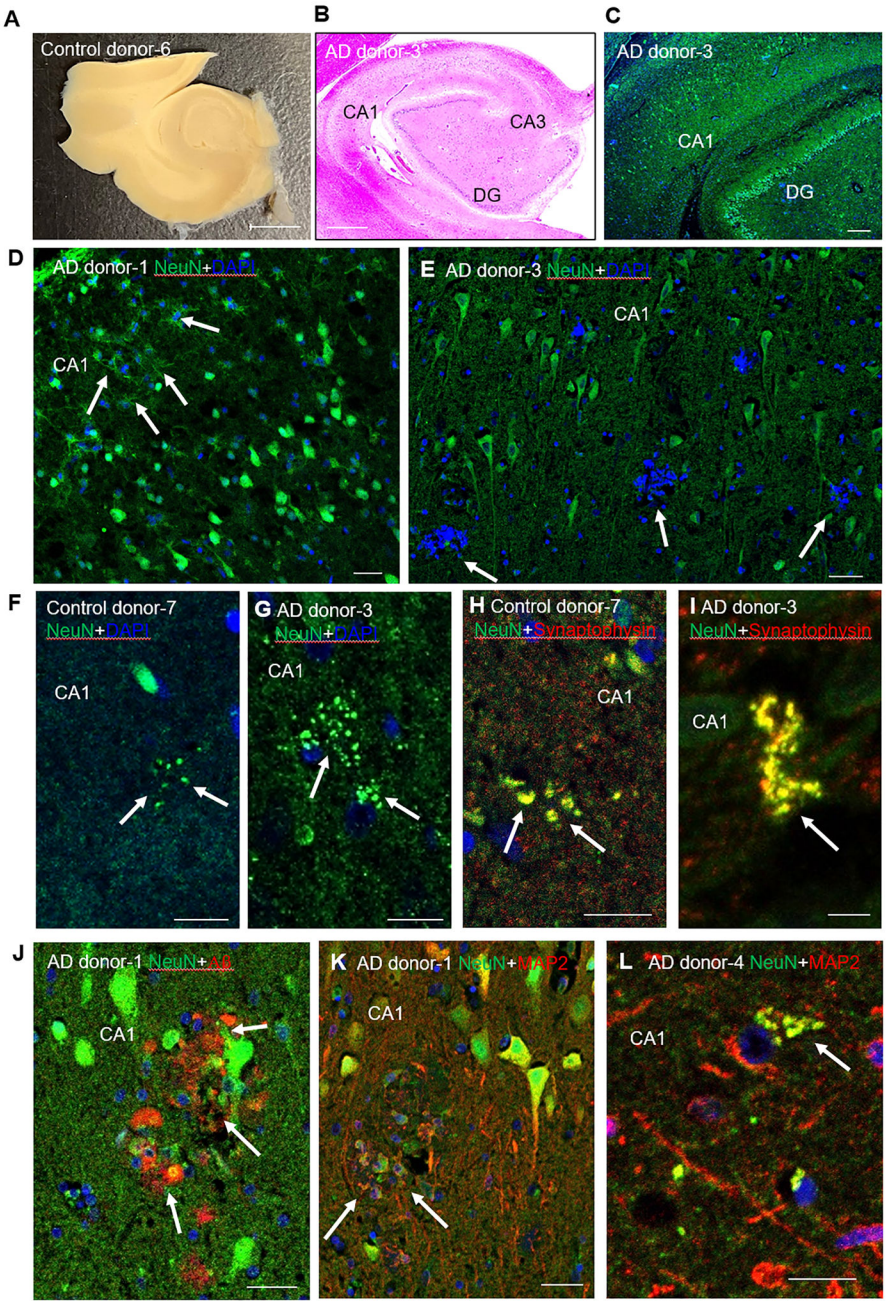


**Figure 7. Human donors with Alzheimer's disease have similar NeuN-labeled structures in hippocampal CA1**

**A**: Human brain tissue (donor 6) including the CA1 hippocampal region. Scale bar:5mm. **B**: Section of human brain (donor 3) stained with H&E (Hematoxylin and Eosin) to identify regions of the hippocampus (CA1 and CA3 and DG as dentate gyrus). Scale bar:1mm. **C**: IF with NeuN labeling (green) to show the hippocampal CA1 region of a human brain section (donor 3). Scale bar:200μm**. D**: IF with NeuN labeling in the CA1 of the late-stage AD donor 1 shows remnants of degenerated neurons (arrows) along with normal-looking neurons. Scale bar:20μm. **E**: IF with NeuN labeling in the CA1 of donor 3 with late onset AD. DAPI labeling shows abnormal clusters of unidentified cells (arrow). Scale bar:50μm.

**F-I:** NeuN+ clusters of puncta are found in both control (donor 7; Fig. 7F,H) and in AD brain (donor 3; Fig. 7G,I). Clusters of puncta look similar to the NeuN+ clusters (green IF) of large puncta described in aging DPP6-KO mice. **H,I**: IF for NeuN+ clusters of large puncta (arrows) show colocalization with the presynaptic marker synaptophysin (red) in both the control (H) and AD brain (I). Scale bar:10μm, (F-G). **J**: Aβ-plaques are found in donor 1 by IF with Aβ (red); these plaques also show partial colocalization with NeuN (green) labeling (arrow). **K,L**: IF in AD brain donors 1 (K) and 4 (L) with MAP2 (red) and NeuN (green) labeling shows some distinctly labeled apical dendrites and irregular clusters of NeuN+ small-cells and processes surrounded with MAP2 (arrow in K) and overlap of red and green labeling in an NeuN+ cluster of puncta (arrow in L). Scale bar=50μm, (H-I).

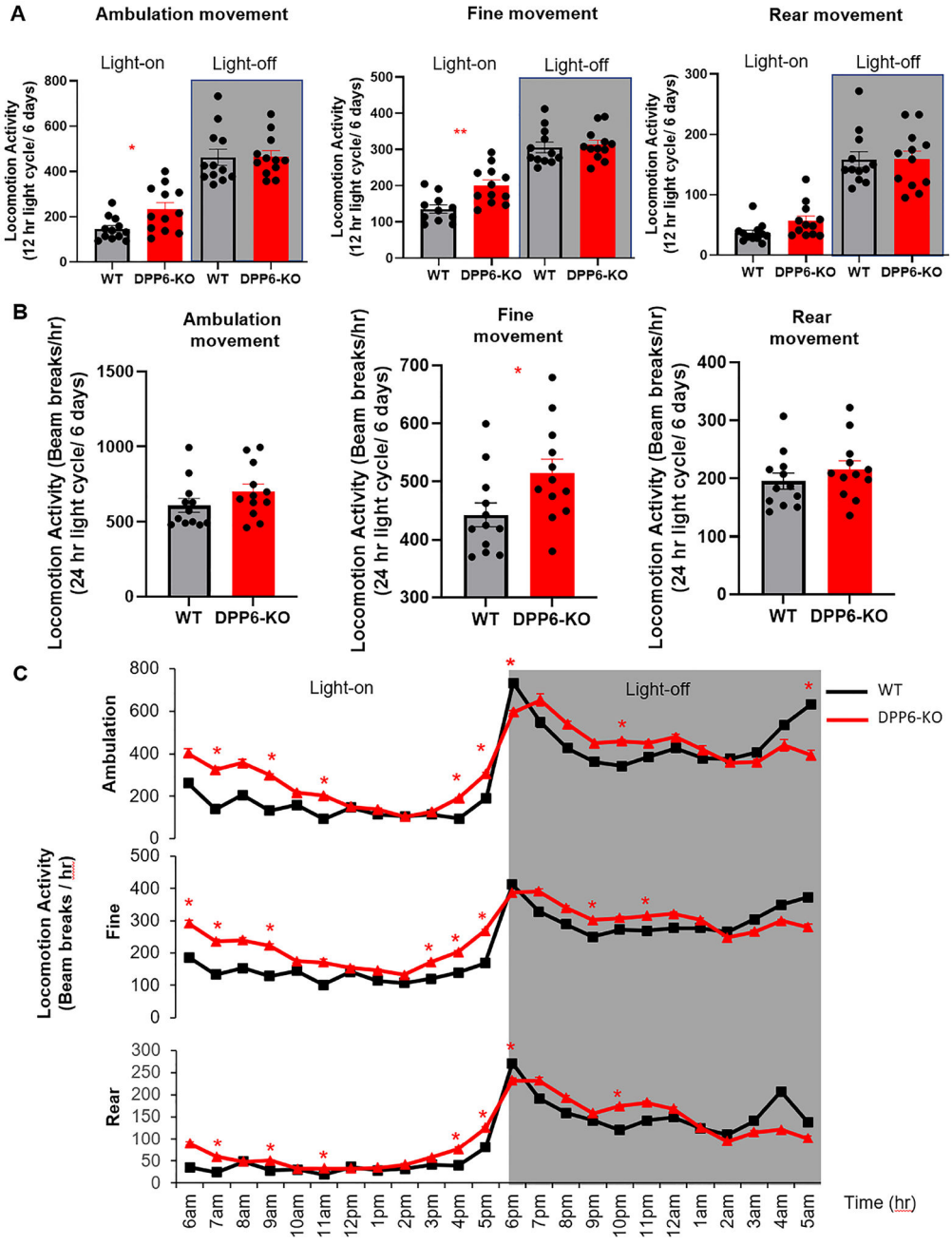


**Figure 8. Aging DPP6-KO mice show circadian rhythm disruption**

**A**: 12-month DPP6-KO have significantly higher locomotor activities compared to WT for the measurement of ambulation and fine movements (n=12 mice each, Two-way ANOVA, $p$ <0.05, $p$ <0.01), but not in rear movements during the Light-on phase (Two-way ANOVA, $p$> 0.05), and no significant increase during the Light-off phase (Two-way ANOVA, $p$ >0.05). **B**: With pooled Light-on and Light-off times, fine movement activity of DPP6-KO mice is significantly increased compared to WT (n=12 mice each, Student's t-test, $p$ <0.05), but there are no differences in ambulation movement or rearing activity (Student's t-test, $p$ >0.05). **C**: With the hourly activity of Light-on and Light-off in three movements, the

circadian rhythm/clock is off at certain time points, especially in Light-on, in DPP6-KO mice compared to WT (n=12 mice each, Student's t-test, $p$ <0.05). Error bars represent ±SEM. Statistical significance was evaluated by Student's t test or two-way ANOVA with Tukey's multiple comparisons. *$p$ < 0.05, **$p$ < 0.01, ***$p$ < 0.001.